Journal of Analytical and Applied Pyrolysis 177 (2024) 106328

Contents lists available at ScienceDirect

Journal of Analytical and Applied Pyrolysis

journal homepage: www.elsevier.com/locate/jaap

The implication of kinetics characteristics of modern organisms for the hydrocarbon generation evolution of organic matter components in the lacustrine source rocks: A case study of the Dongying Formation from the Bozhong Sag, Bohai Bay Basin

Guoxiong Li [a,b,e], Chenglin Liu [a,b,*], Rizwan Sarwar Awan [c], Xiaoyi Yang [a,b], Dehao Feng [a,b], Feilong Wang [d], Xiaoxiang Zeng [a,b], Hong Yang [a,b], Jiajia Su [a,b], Yuping Wu [a,b], Taozheng Yang [a,b], Zhen-gang Ding [a,b], Zhangxing Chen [e]

[a] National Key Laboratory of Petroleum Resources and Engineering, China University of Petroleum (Beijing), Beijing 102249, China
[b] College of Geosciences, China University of Petroleum (Beijing), Beijing 102249, China
[c] School of Resources and Environmental Engineering, Hefei University of Technology, Hefei 230009, China
[d] Tianjin Branch of CNOOC China Limited., Tianjin 300452, China
[e] Department of Chemical and Petroleum Engineering, University of Calgary, Calgary, AB, T2N 1N4 Canada

ARTICLE INFO

Keywords:
Lacustrine source rocks
Pine pollen
Benthic algae
Hydrocarbon generation kinetics
Thermal and basin simulation
Bozhong Sag

ABSTRACT

The hydrocarbon generation evolution characteristics of lacustrine source rocks are crucial for understanding hydrocarbon resources. In this research, we focus on the mudstone found in the third member of the Paleogene Dongying Formation (E_3d_3) within the Bozhong Sag of the Bohai Bay Basin as a case study. An analysis of the discrepancy in geochemical characteristics and kinetic parameters was carried out by utilizing the modern organisms (pine pollen and benthic algae) analogies to the organic matter (OM) components (Pinaceae sporopollen and benthic algae amorphous). Furthermore, the bulk hydrocarbon evolution of the Dongying Formation mudstones was further discussed in combination with a water-added sealing thermal simulation experiment and basin simulation. Our findings indicate that the pine pollen and benthic algae have higher OM abundance compared to the E_3d_3 mudstones, and their OM types are both II_1-II_2, which possess excellent potential for oil generation. In contrast, the E_3d_3 mudstones are predominantly in the low mature to mature thermal evolution stage. When we compare hydrocarbon generation rates and transformation ratios using Rock-Eval pyrolysis, it becomes evident that modern organisms are more prone to generate large amounts of hydrocarbons even at a low mature stage. The kinetic parameters of pine pollen are notably higher compared to those of benthic algae and the E_3d_3 mudstone samples. In parallel first-order reactions, the activation energy obtained by the single-frequency factor model (SFFP model) displays a narrow distribution range, while the activation energy distribution range of the multi-frequency factor model (MFFP model) is broader. The MFFP model focuses more on the variations of hydrocarbon kinetic parameters throughout the entire process, which is more in conformity with the actual geological process. The enclosed thermal simulation experiment and basin simulation analysis unveil the presence of two distinct phases of hydrocarbon generation within the Dongying Formation. Furthermore, it becomes evident that abundant benthic algae and Pinaceae sporopollen components play vital roles in both of these phases. In conclusion, the method of applying modern organisms to analogize the hydrocarbon generation evolution characteristics of the parent components of lacustrine source rocks seems feasible. Meanwhile, the Dongying Formation in the Bozhong Sag also possesses broad exploration prospects for hydrocarbon resources.

* Corresponding author at: National Key Laboratory of Petroleum Resources and Engineering, China University of Petroleum (Beijing), Beijing 102249, China.
E-mail address: lclzgx@126.com (C. Liu).

https://doi.org/10.1016/j.jaap.2023.106328
Received 15 October 2023; Received in revised form 3 December 2023; Accepted 22 December 2023
Available online 23 December 2023

1. Introduction

The theory of hydrocarbon generation through late thermal degradation of kerogen has significantly and effectively guided the majority of oil and gas exploration projects [1]. On this basis, numerous researchers have conducted extensive studies on the formation mechanism of hydrocarbons in the immature to low mature stages, which have advanced and promoted our understanding of hydrocarbon genesis theory [2–4]. Sedimentary OM serves as the material foundation for hydrocarbon generation and plays an essential role in the process of hydrocarbon formation. Some scholars have focused on the influence of parent components for hydrocarbon generation in source rocks. Predecessors have conducted experimental analyses with various organisms and OM components, such as Pinaceae sporopollen [5–8], benthic and planktonic algae [9–12], Scenedesmus algae [13], telalginite and lamalginite [14], and amorphous OM [15] to study hydrocarbon generation processes. Their findings showed remarkable distinctions in the hydrocarbon generation potential, activation energy, generation evolution process, and the characteristics of the resulting products at different temperature (maturity) stages of various components.

Kinetic analysis is crucial for studying the hydrocarbon generation process and the mechanism of organic components. Based on the principle of temperature and time compensation, the thermal evolution and hydrocarbon generation characteristics of OM can be rapidly obtained under laboratory conditions [16,17]. Hydrocarbon generation from OM is a complex compositional kinetic process that involves the cracking of covalent bonds of numerous OM molecules and variations in the required activation energy [16,18–20]. By comparing several chemical kinetic models, the predecessors believed that the parallel first-order reaction model is widely representative and applicable for describing the hydrocarbon generation process [21–23]. The discrepancies in the process are characterized by three obtained kinetic parameters (activation energy, frequency factor, and reaction fraction). Additionally, the parallel first-order reaction can be divided into a single-frequency factor model (SFFP model) and a multi-frequency factor model (MFFP model). The SFFP model is highly simplified and may potentially result in an inaccurate assessment of the hydrocarbon generation characteristics of OM. In contrast, the MFFP model can better describe the entire evolutionary process of hydrocarbon generation [18,21]. A comparative analysis of kerogen discrete activation energy results obtained through single and multiple pyrolysis heating ramps in the open system has been carried out by previous studies [24–26]. It was considered that the activation energy distribution derived from a single heating ramp may be unreliable, as the influence of a fixed frequency factor could be offset during the adjustment of average activation energy, but that the temperature errors would be amplified when applied to geological simulation [25]. In contrast, employing multiple heating ramps and a dynamically optimized frequency factor model yields more accurate kinetic parameters [27]. Additionally, the comprehensive reconstruction of the hydrocarbon generation history of OM under geological conditions can be achieved by integrating basin simulation technology with stratigraphic, geochemical, and kinetic parameters [22,28–30].

The Bozhong Sag is the largest hydrocarbon-rich sag in the Bohai Bay Basin, with proven and discovered large-scale oil and gas fields widely distributed in the vicinity of the sag [31–35]. The hydrocarbon formation mechanism of source rocks in offshore intricate geological conditions has attracted considerable attention. Previous studies primarily concentrated on the Paleogene Shahejie Formation in Bozhong Sag and identified the contribution of this set of source rocks to hydrocarbon accumulation [33,36]. However, the understanding of the hydrocarbon generation evolution of source rocks in the Dongying Formation is not profound enough. Previous studies have suggested that the origin of OM in the Dongying Formation is predominantly mixed sources, with both terrestrial plant inputs and contributions from lower aquatic organisms [36,37]. During the bottom-up deposition process, the quality of source rocks gradually deteriorated. Among them, the E_3d_3 interval has deposited a set of thick high-quality source rocks with high OM abundance. The average total organic carbon content (TOC) is approximately 2%, and the hydrocarbon generation potential typically exceeds 6 mg/g, predominantly attributed to type II kerogen, which is in the middle and low maturity stage and indicates a favorable hydrocarbon generation capacity [31]. The benthic algal amorphous content (10%−43%) and Pinaceae sporopollen content (12.9%−77.8%) within the hydrocarbon generation components of the Dongying Formation hold specific advantages and make significant contributions to hydrocarbon generation at both low mature and mature stages [37]. However, the previous study only analyzed the relationship between the statistical content of the two components and the hydrocarbon generation potential of the Dongying Formation at different thermal maturity stages, and the relevant kinetic and thermal simulation studies have not been carried out. In order to further verify the hydrocarbon generation evolution characteristics of the two special components, this study adequately employed pine pollen and benthic algae (laver) analogous to the hydrocarbon generation components, and carried out the comparison of organic geochemical characteristics and kinetic parameters, thermal simulation experiment, and basin simulation analysis. The paper discusses discrepancies in the regularity of hydrocarbon generation evolution and kinetic characteristics of modern organisms and the E_3d_3 interval mudstones under various models. Its primary objective is to explore the feasibility of using modern organisms as analogous for hydrocarbon generation components and to enhance the understanding of the hydrocarbon generation mechanism of source rocks in the Dongying Formation.

2. Geological setting

The Bohai Bay Basin is an important oil and gas basin in eastern China. It is a typical Cenozoic continental faulted lacustrine basin with an area of about 20×10^4 km^2 (Fig. 1a) and contains rich oil and gas resources [31,34,38]. The Bozhong sag is located in the Bohai Sea, surrounded by Shijiutuo, Shaleitian, Chengbei, Bonan, Bodong, and other uplifts, with an area of 8634 km^2 (Fig. 1a). This study focuses on the mudstones within the Dongying Formation of the Paleogene Oligocene, which serves as a vital source rock series (Fig. 1b). The Dongying Formation is divided into three members from bottom to top: the third member (E_3d_3), the second member (E_3d_2) and the first member (E_3d_1). In the Paleogene Oligocene (E_3), the tectonic evolution of the basin belongs to the late stage of rifting and gradually transforms into the post-rift thermal subsidence stage [39–41]. During the sedimentary period of the Dongying Formation, the basin was in the synrift stage IV. The intense role of fault-depression conversion enabled the subsag area of Bozhong Sag to increase its accommodation space and accelerate the deposition rate of sediments. Sedimentary facies in the subsag areas mainly developed from deep lake to semi-deep lake and shallow lake, and the uplift areas and slope transition zones were mostly deposited by the river delta (Fig. 1). Overall, the Dongying Formation was primarily formed in a lacustrine-delta depositional environment with sulfur-poor in freshwater, open and rich-clay, and insignificant water column stratification, which is characterized by typical weak oxidation-reduction sedimentary conditions [36]. In the bottom-up depositional process, the terrestrial input gradually intensified, hence the upper sub-member of E_3d_2 and the E_3d_1 were dominated by sandstone and mudstone interbeds with poor-quality source rocks. In contrast, thick gray-dark brown mudstones were widely developed in the E_3d_3 and the lower sub-member of E_3d_2. Especially in the E_3d_3 interval, which formed a set of high-quality organic-rich lacustrine source rocks owing to favorable preservation conditions.

3. Samples and methods

In this study, a total of thirty-three mudstone samples of the E_3d_3 interval were collected from six wells in the Bozhong Sag, two modern organisms (pine pollen and benthic algae), and one mixed sample

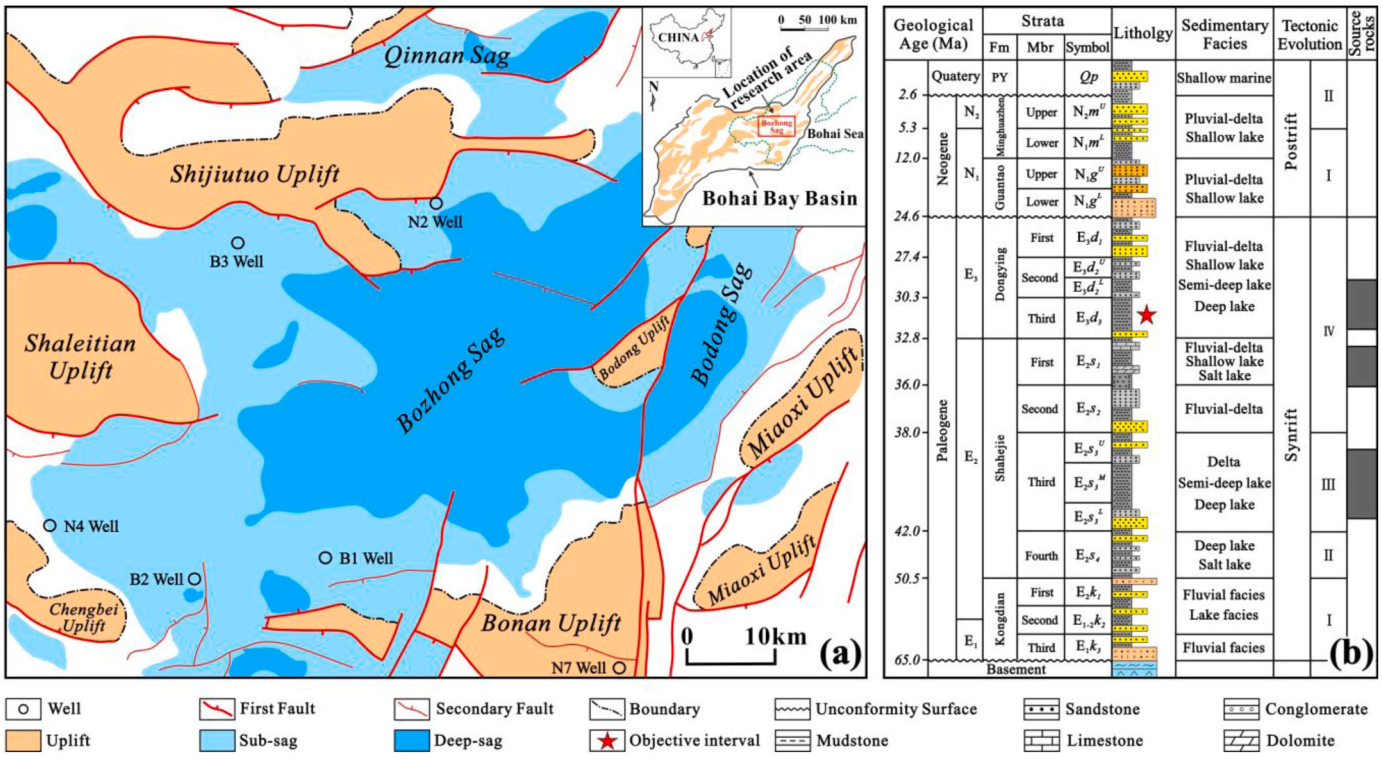

Fig. 1. (a) Map showing tectonic units and locations of studied wells in the Bozhong Sag, Bohai Bay Basin; (b) Cenozoic stratigraphic column of the Bozhong Sag (modified from [31]). PY=Pingyuan; N_2 =Pliocene; N_1 =Miocene; E_3 =Oligocene; E_2 =Eocene; E_1 =Paleocene; Fm=Formation; Mbr=Member.

(H18–1) for organic geochemical experiments, hydrocarbon generation kinetics analysis, and thermal simulation in the autoclave (Fig. 1, Fig. 2, Table 1). Pine pollen originates from the northeastern region of China and belongs to the gymnosperm pollen of higher plants. It appears as a light yellow powder with semi-circular symmetrical network air sac structures on both sides (Fig. 2a). At the low maturity stage, the elemental composition of pine pollen includes 71.92% C, 6.84% H, 10.47% O, and 3.99% N, and the H/C and O/C were 1.33 and 0.11 [8]. There are oil bodies in pine pollen grains, indicating they as a favorable precursor for oil generation [42]. Benthic algae (laver) source from the Bohai Sea, presents itself as dark green to purple-black sheet-like morphology (Fig. 2b). Previous studies showed that the contents of C, H, O, N, and S elements in benthic algae were 36.88%, 4.18%, 44.41%, 5.81%, and 2.43%, respectively, with H/C and O/C were 2.95 and 0.90 [11]. The lipid and protein contents of benthic algae (laver) can reach 1.96% and 32.16%, respectively [43]. Furthermore, the mixed sample (H18–1) refers to the uniform mixing of three 100-mesh fineness powder samples of the E_3d_3 mudstone (N4–11), pine pollen, and benthic algae (laver) at a mass ratio of 18:1:1. Whereby, the H18–1 sample consists of a mixture of wt.90% mudstone, wt.5% pine pollen and wt.5% benthic algae.

3.1. TOC and Rock-Eval pyrolysis

The selected samples were initially crushed and grounded to a very fine mesh size (<100). Afterward, they were subjected to a treatment using a diluted solution of hydrochloric acid (5%) at a constant temperature of 80 ℃ to eliminate carbonate minerals. Following this, the samples underwent multiple rinses with deionized water before being dried in an 80 ℃ oven for 12 h. Finally, the samples were fully combusted on the CS-902 high-frequency infrared carbon-sulfur analyzer, and the TOC content was obtained by detecting the product. The Rock-Eval VI device was used for pyrolysis analysis. Each powdered sample (100 mg) was first placed in a helium atmosphere to remove air before loading into a combustion dish. After starting heating, the samples were heated at a temperature programmed at 300 ℃ for 3 min to obtain free hydrocarbons (S_1, mg HC/g Rock). Then, the temperature was continued to increase to 600 ℃ at a rate of 25 ℃/minute to determine the pyrolysis

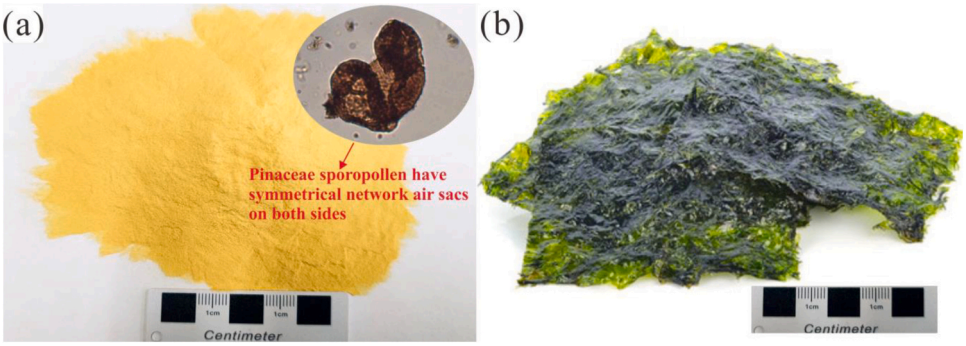

Fig. 2. Sample of modern organisms components, (a) pine pollen; (b) benthic algae (laver).

Table 1
Basic geochemical test data of modern biological and mudstone samples from the third member of the Dongying Formation (E_3d_3).

Well	Samples	Depth (m)	Types	TOC (wt %)	S_1 (mg/g)	S_2 (mg/g)	T_{max} (℃)	GP (mg/g)	PI	HI (mg/g)	GPI (mg/g)	R_o (%)	R_c (%)	Sapropelinite (%)	Exinite (%)			Vitrinite (%)	Inertinite (%)	TI	OM types
															BAA	Other	Total				
B1	B1-1	4575	mudstone	1.99	1.63	5.70	426	7.33	0.22	286.00	368.34	0.90	0.52	16	16	58	74	7	3	44.8	II_1
	B1-2	4615	mudstone	1.99	1.60	4.62	432	6.22	0.26	232.00	312.56	0.93	0.62	19	15	55	70	10	1	45.5	II_1
	B1-3	4715	mudstone	3.04	1.63	3.47	428	5.10	0.32	114.00	167.76	0.98	0.55	19	16	49	65	11	5	38.3	II_2
	B1-4	4845	mudstone	1.46	0.63	2.74	435	3.37	0.19	188.00	230.82	1.03	0.67	19	20	50	70	10	1	45.5	II_1
	B1-5	4895	mudstone	2.41	0.96	3.00	425	3.96	0.24	124.00	164.32	1.05	0.50	19	13	56	69	10	2	44	II_1
B2	B2-1	3795	mudstone	0.95	0.42	2.80	440	3.22	0.13	293.68	338.95	0.71	0.75	30	19	42	61	7	2	53.3	II_1
	B2-2	3875	mudstone	1.03	0.56	2.73	437	3.29	0.17	265.05	319.42	0.74	0.70	33	24	30	54	12	1	50	II_1
	B2-3	3925	mudstone	1.55	0.90	5.12	441	6.02	0.15	328.39	388.39	0.76	0.77	25	20	40	60	14	1	43.5	II_1
	B2-4	3975	mudstone	1.84	1.26	6.63	441	7.89	0.16	360.87	428.80	0.80	0.77	27	15	46	61	10	2	48	II_1
	B2-5	4025	mudstone	2.60	1.33	9.73	442	11.06	0.12	372.69	425.38	0.79	0.78	21	14	56	70	8	1	49	II_1
	B2-6	4075	mudstone	2.78	1.02	10.33	443	11.35	0.09	371.58	408.27	0.84	0.80	17	16	55	71	10	2	43	II_1
B3	B3-1	3405	mudstone	1.90	0.99	4.40	436	5.39	0.18	232.00	283.68	0.73	0.68	8	34	46	80	5	7	37	II_2
	B3-2	3435	mudstone	1.32	0.74	4.53	435	5.27	0.14	343.00	399.24	0.70	0.67	6	50	36	86	5	3	42	II_1
	B3-3	3485	mudstone	1.83	1.11	5.55	435	6.66	0.17	303.00	363.93	0.70	0.67	7	44	41	85	4	4	43	II_1
	B3-4	3515	mudstone	1.62	0.81	4.52	435	5.33	0.15	279.00	329.01	0.71	0.67	6	33	54	87	4	3	44	II_1
	B3-5	3545	mudstone	2.09	1.45	5.76	441	7.21	0.20	276.00	344.98	0.66	0.77	4	29	56	85	5	6	37	II_2
	B3-6	3575	mudstone	1.66	0.69	5.31	442	6.00	0.12	320.00	361.45	0.67	0.78	6	23	62	85	4	5	41	II_1
	B3-7	3625	mudstone	1.81	0.61	6.34	442	6.95	0.09	350.00	383.98	0.72	0.78	13	19	63	82	4	0	52	II_1
N2	N2-5	3915	mudstone	1.14	0.47	3.47	445	3.94	0.12	304.00	345.61	0.72	0.83	35	15	46	61	3	1	63	II_1
	N2-6	3945	mudstone	1.00	1.05	2.78	444	3.83	0.27	278.86	384.19	0.70	0.82	34	37	26	63	2	1	64	II_1
	N2-7	3975	mudstone	1.88	0.89	6.45	442	7.34	0.12	343.00	390.43	0.76	0.78	40	21	35	56	3	1	66	II_1
	N2-8	3985	mudstone	1.89	1.02	6.56	442	7.58	0.13	347.00	401.06	0.70	0.78	39	20	38	58	2	1	66	II_1
	N2-9	3995	mudstone	2.00	1.10	7.45	442	8.55	0.13	373.00	427.50	0.78	0.78	33	23	40	63	3	1	62	II1
N4	N4-8	3095	mudstone	1.02	0.33	2.99	439	3.32	0.10	294.12	325.49	0.74	0.73	21	24	35	59	16	4	34.5	II_2
	N4-9	3135	mudstone	0.99	0.37	3.01	438	3.38	0.11	303.03	341.41	0.76	0.72	26	25	33	58	14	2	42.5	II_1
	N4-10	3175	mudstone	2.71	1.03	13.74	439	14.77	0.07	507.01	545.02	0.75	0.73	27	38	25	63	9	1	50.8	II_1
	N4-11	3215	mudstone	3.96	3.54	20.33	440	23.87	0.15	513.38	602.78	0.77	0.75	26	33	29	62	10	2	47.5	II_1
	N4-12	3255	mudstone	3.98	2.99	21.94	440	24.93	0.12	550.75	626.38	0.82	0.75	35	20	31	51	12	2	49.5	II_1
N7	N7-3	1950	mudstone	0.90	0.91	3.25	435	4.16	0.21	361.11	462.22	/	0.67	21	24	48	72	7	1	51	II_1
	N7-4	1980	mudstone	2.16	2.26	11.54	431	13.80	0.16	534.25	638.89	/	0.60	11	21	55	76	11	2	39	II_2
	N7-5	2010	mudstone	2.15	4.90	10.61	438	15.51	0.32	493.49	721.40	/	0.72	23	15	53	68	8	1	50	II_1
	N7-6	2040	mudstone	2.31	2.65	14.60	436	17.25	0.15	632.03	746.75	/	0.68	19	10	64	74	6	1	51	II_1
	N7-7	2070	mudstone	2.60	2.34	16.21	434	18.55	0.12	623.46	713.46	/	0.65	24	10	58	68	7	1	52	II_1
/	H18-1	/	mixed sample	6.32	21.22	31.76	430	52.98	0.40	502.53	838.29	/	0.59	/	/	/	/	/	/	/	/
/	SF1-2	/	pine pollen	29.33	128.13	141.64	408	269.77	0.47	482.94	919.82	/	0.22	/	/	/	/	/	/	/	/
/	ZC1-1	/	benthic algae	13.80	81.24	52.39	399	133.63	0.61	379.64	968.34	/	0.07	/	/	/	/	/	/	/	/

TOC: total organic carbon; S_1: free hydrocarbons; S_2: pyrolysis hydrocarbons; T_{max}: the temperature of the S_2 hydrocarbon peak; GP=S_1 +S_2, hydrocarbon generation potential; PI=S_1/(S_1 +S_2), production index; HI=S_2/TOC× 100, hydrogen index; GPI= (S_1 +S_2)/TOC, generation potential index; %R_c = 0.0165 ×T_{max}- 6.51 (Jarvie, 2018), BAA=benthic algal amorphous; TI=sapropelinite+ 0.5 ×exinite-0.75 ×vitrinite-inertinite, type index; "/", no data.

hydrocarbon (S_2, mg HC/g Rock) and the highest pyrolysis peak temperature (T_{max}, ℃) in this stage.

3.2. Vitrinite reflectance (R_o) and maceral composition

The thin sections of the selected fresh rock samples were prepared by embedding them in epoxy resin, dried, and polished until the surface was smooth to create a whole rock-light sheet. The R_o values of vitrinite were measured with an optical microscope (188 MPV-SP) at a wavelength (λ) of 546 nm ± 5 nm using the oil immersion method. The measurements were carefully calibrated several times to obtain the average R_o value for each sample. The kerogen macerals were observed and identified utilizing the LEICA DM4500 microscope with transmission and reflectance fluorescence functions. Finally, the quantitative statistics of each maceral were carried out by percentage content.

3.3. Kinetics analysis

The Rock-Eval VI device was employed for conducting experiments on the kinetics of hydrocarbon generation in mudstone and modern biological samples. Initially, a powder sample (100 mg) was placed in a combustion dish, and four parallel samples were prepared for each sample holder. To initiate the experiment, the samples underwent an initial heating step, reaching a temperature of 200 ℃, which was maintained for 3 min to eliminate any adsorbed hydrocarbons on the samples. Subsequently, each sample followed a temperature programmed with four distinct heating rates (10, 30, 40, and 50 ℃/min) from 200 ℃ to 600 ℃. Flame ionization detection (FID) was performed on the pyrolysis products in a helium atmosphere to obtain the cumulative hydrocarbon generation conversion curves at different temperature rates. The kinetic characteristics of parallel reactions were analyzed according to the Arrhenius principle [16,44]. Finally, we obtained distribution results of discrete activation energy, frequency factor, and reaction fraction using KINETICS 2015 software with the SFFP and MFFP models. Here, the SFFP model refers to the application of a fixed single-frequency factor in the parallel first-order reaction model, which relies on the average frequency factor to encompass all phases of the parallel reaction. The MFFP model refers to a parallel first-order reaction model with multiple frequency factors, where each obtained activation energy corresponds to an optimized frequency factor.

3.4. Thermal simulation experiment

The thermal simulation experiment for hydrocarbon generation with closed water addition on the mixed sample (H18–1) was conducted using an autoclave device. Initially, nine parallel samples were prepared, each with a mass of 10 g per portion. The sample was put into the autoclave and about 10 ml of deionized water was added to fully immerse the sample. Subsequently, the reactor body was sealed, vacuumed, and then heated. The research aimed to achieve specific temperatures for experiments, including 200 ℃, 250 ℃, 300 ℃, 320 ℃, 340 ℃, 355 ℃, 370 ℃, 400 ℃, and 450 ℃. Once these target temperatures were reached, they were kept constant for 48 h. Finally, the experimental products were collected, and the liquid hydrocarbon and gas products were obtained by methylene chloride extraction and saturated NaCl solution drainage and gas collection, respectively. The liquid hydrocarbons were separated by alumina/silica gel column chromatography to obtain the mass percentage of saturated hydrocarbons, aromatics, heterocompounds, and asphaltenes. Concurrently, the composition of gaseous products was also analyzed to distinguish non-hydrocarbon gases. Additionally, the oil production rate and the volume of hydrocarbon gas production were quantified.

3.5. Basin modeling

The history of burial, thermal, and hydrocarbon generation evolution of the Dongying Formation source rocks in the Bozhong Sag was reconstructed using the PetroMod@ 2016 1D software. The lithology and thickness of the formation were determined based on the logging data from the study wells, and the geological age is illustrated in Fig. 1b. The absolute ages of stratigraphic unconformities and erosion events, along with the recovery of erosion amount were referenced from published works [45,46]. Boundary conditions included paleo-water depth (PWD), sediment-water interface temperature (SWIT), and heat flow (HF) [47]. The determination of PWD relied on previous calculations utilizing cobalt and lanthanum elemental [48]. SWIT during deposition was calibrated based on Wygrala's study of global paleo-surface temperatures [49], considering the location of the Bohai Bay Basin (38°N). The distribution of HF was referenced in the research results of Hu [50] and Qiu [51,52]. We performed the EASY %R_o model with measured R_o values serving as constraints to calibrate the thermal evolution simulation results. The hydrocarbon generation from the Dongying Formation obeyed the kinetic pattern obtained under the SFFP or MFFP models.

4. Results and discussion

4.1. Bulk geochemical characteristics

There are remarkable differences in the OM abundance between the source rocks of the Dongying Formation and modern organisms (Table 1). The TOC content, S_1, S_2, and hydrogen index (HI=S_2/TOC×100) of the analyzed samples from the E_3d_3 interval are 0.90%− 3.98% (average 1.96%), 0.33–4.90 mg/g (mean 1.34 mg/g), 2.73–21.94 mg/g (averaging 7.22 mg/g), and 114.00–632.03 mg/g (meaning 348.42 mg/g). The mixed sample (H18–1), pine pollen, and benthic algae (laver) have higher TOC contents, which are 6.32%, 29.33%, and 13.80%, respectively. The HI values for these samples are 502.53 mg/g, 482.94 mg/g, and 379.64 mg/g, respectively. However, the S_1 (128.13 mg/g) and S_2 (141.64 mg/g) values of the pine pollen are the highest among all the other samples (Table 1). The hydrocarbon generation potential (GP=S_1 +S_2) value of modern organisms (average 201.70 mg/g) is higher than that of the mixed sample (52.98 mg/g) and the E_3d_3 mudstones (mean 8.56 mg/g).

The distribution of TOC, GP, and HI can reflect discrepancies in the hydrocarbon generation potential of OM [1,53–55]. The positive correlation between TOC and GP content designates that the E_3d_3 interval has good to excellent-quality source rock properties, while both modern organisms and mixed sample (H18–1) exhibit excellent-quality characteristics (Fig. 3a). Moreover, the hydrocarbon generation potential index [GPI= (S_1 +S_2)/TOC] of the E_3d_3 mudstone samples is 164.32–746.75 mg/g, with an average of 414.91 mg/g. However, the GPI of the modern organisms and mixed sample are higher, with a mean of 908.82 mg/g (Table 1). The cross plot of TOC and HI also confirms that the E_3d_3 mudstones, pine pollen, benthic algae, and mixed sample possess good oil generation potential (Fig. 3b).

The composition of macerals can be used to determine the type of OM [1,56,57]. Statistical results show that the exinite comprises the largest proportion within the source rocks of the Dongying Formation, ranging from 51%− 87% (average 68.7%), in which the content of benthic algae amorphous (BAA) can reach 10%− 50% (average 22.91%) (Table 1). The morphology of BAA observed under the microscope was mostly flocculent and clumpy (Fig. 4a, b). It is generally formed by the degradation of benthic macroalgae and plays a vital role in the process of hydrocarbon generation [37]. Followed by the sapropelinite content of 4%− 40% (mean 21.48%). In contrast, the vitrinite and inertinite content are smaller, with an average of 7.67% and 2.15%, respectively (Table 1).

Previous studies and statistics have shown that the source rocks of the Dongying Formation in the Bozhong Sag are rich in sporopollen paleontology [37]. The sporopollen mainly contains four types: algae, ferns, angiosperms, and gymnosperms. The content of gymnosperms in

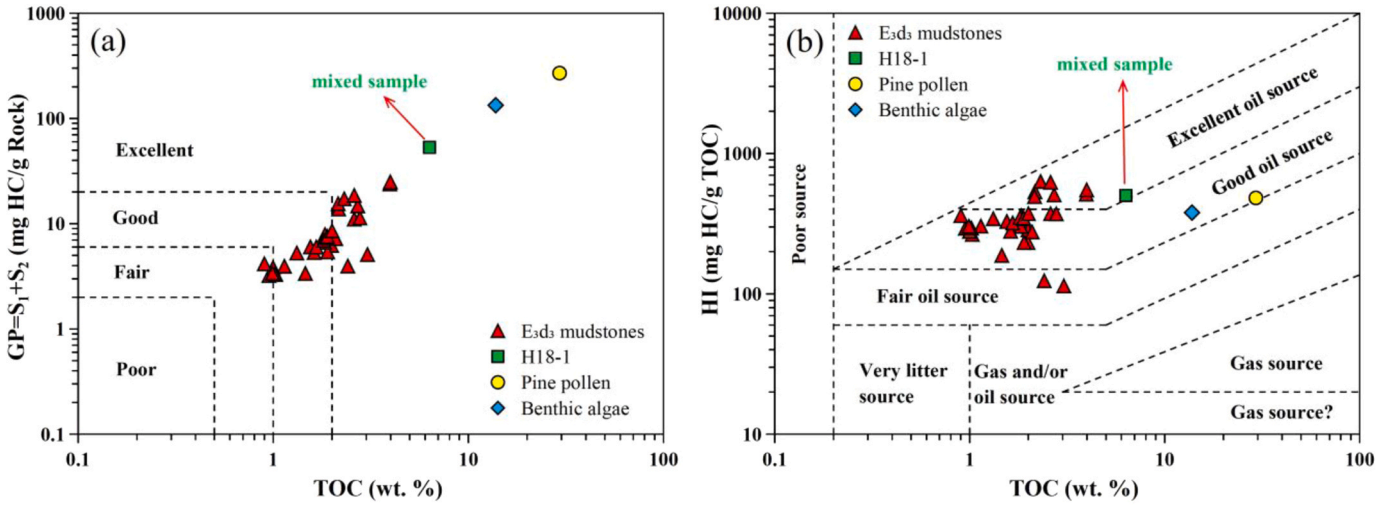

Fig. 3. Evaluation of OM abundance for the studied samples, showing excellent oil generation potential. (a) Cross plot of TOC and GP (according to [1]); (b) Relationship between TOC and HI (according to [53]).

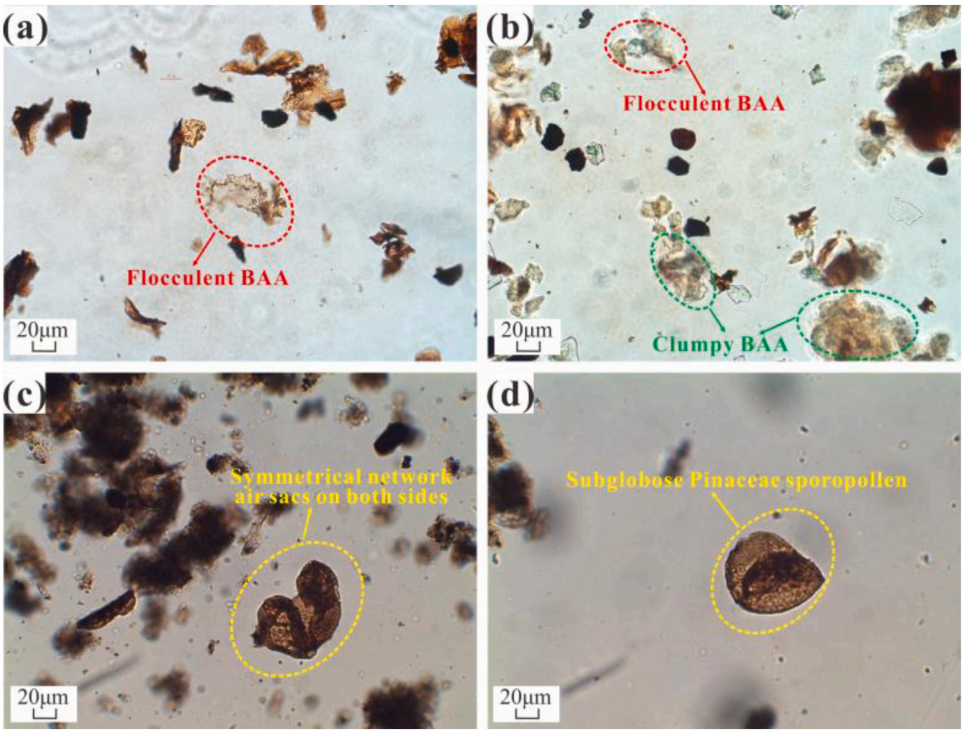

Fig. 4. Characteristics of benthic algae amorphous (BAA) and Pinaceae sporopollen of the Dongying Formation from Bozhong Sag [37]. (a) flocculent BAA, 3695 m; (b) flocculent and clumpy BAA, 4345 m; (c) Pinaceae sporopollen have symmetrical network air sacs on both sides, 3545 m; (d) subglobose Pinaceae sporopollen, 3565 m.

the mudstones of the E_3d_3 interval is the highest, ranging from 15.5%–92.4% (average 50.6%), especially the single/double-bundle pine pollen from Pinaceae is 12.9%– 77.8% (mean 30.7%), which are the dominant constituent of gymnosperms (Fig. 5). The morphology of the Pinaceae sporopollen was observed under the microscope to be almost subglobose, with symmetrical network air sacs on both sides (Fig. 4c, d). These sporopollen are essential components of the parent material of source rock, and the difference in its content also affects the evolutionary process of hydrocarbon generation[5,6].

The ternary diagram of maceral composition shows that the E_3d_3 mudstones are mainly comprised of mixed OM (type II) (Fig. 6a). The types of OM can be divided into four categories based on the kerogen type index (TI=sapropelinite+0.5 ×exinite-0.75 ×vitrinite-inertinite), and the larger the TI value, the better the OM type [30]. The TI values of the tested samples from the E_3d_3 interval range from 34.5 to 66.0, with an average of 48.17, proving that the OM types of the Dongying Formation are mainly type II_1-II_2 (Table 1, Fig. 6b). Furthermore, the distribution relationship between T_{max} and HI suggests that the OM types of the E_3d_3 mudstones, pine pollen and benthic algae are mainly type II_1 and II_2 (Table 1, Fig. 6c).

The R_o, T_{max}, and production index (PI) can effectively characterize the thermal maturity level of the examined samples [1,30,56,58]. The measured R_o of E_3d_3 mudstone samples ranges from 0.66% to 1.05%, with an average of 0.78%, and T_{max} varies between 425 ℃ and 445 ℃,

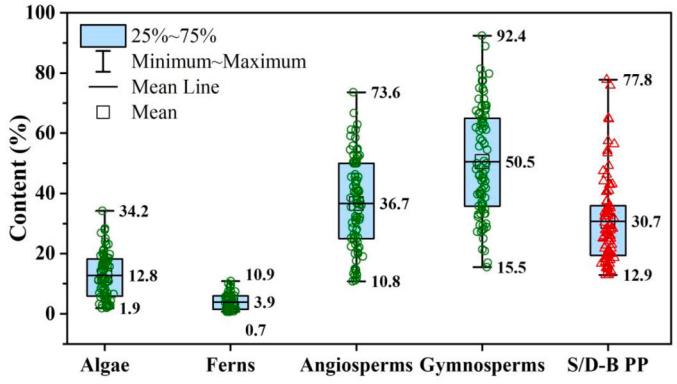

Fig. 5. Box plot of different types of sporopollen content distribution in mudstone of the E_3d_3 interval in the Bozhong Sag (data from [37]). The rounds represent the subpoints of the content data within the four sporopollen components (algae, ferns, angiosperms, and gymnosperms) on the box plot. The triangles represent the content data points of the S/D-B PP (single/-double-bundle pine pollen).

with a mean of 437.6 ℃ (Table 1). It presents that the source rocks are at a low maturity-mature level, and the OM is in the oil window [1]. However, the T_{max} of the mixed sample (H18–1), pine pollen, and benthic algae are 430 ℃, 408 ℃, and 399 ℃, respectively, indicating that these samples belong to the immature stage (Table 1). The positive correlation between R_o and T_{max} has been widely confirmed in marine and lacustrine sediments [30,59,60]. In this study, the relationship between the vitrinite reflectance using Jarvie's (2018) formula (%R_c =0.0165 ×T_{max}-6.51) and T_{max} shows that the equivalent %R_c of modern organisms is 0.22% and 0.07% (Fig. 7a), which is much smaller than the equivalent %R_c of the E_3d_3 mudstones (0.50%−0.83%). The comparison revealed a negative correlation between the measured %R_o and the estimated %R_c (Fig. 7b, R^2 =0.454). This observation differs significantly from the expected results. The investigation found that the R_o values from the B1 well were 0.9% to 1.05%. However, the corresponding T_{max} values were only in the range of 425 ℃ to 435 ℃, resulting in an estimated R_c range of only 0.49% to 0.67%. This discrepancy has caused an error in the thermal maturity assessment (Table 1, Fig. 7b). One potential explanation could be that source rocks with high levels of maturity may retain some hydrocarbon, thereby influencing the pyrolysis process and subsequently impacting the precision T_{max} measurement [61]. Hence, it is advisable to exercise caution when employing the %R_c estimation method for assessing maturity in the mature to highly mature stages. Some researchers have proposed using the post-extraction measured T_{max} value as a more accurate means of evaluating maturity [60]. The PI of the analyzed samples from the Dongying Formation ranged from 0.07–0.32 (average 0.16). In contrast, the PI of H18–1, pine pollen, and benthic algae are 0.4, 0.47, and 0.61, respectively (Table 1, Fig. 7c). It unveils that pine pollen and benthic algae have not undergone diagenesis, and their biomass contains high amounts of free hydrocarbons. The cross plot of PI and T_{max} presents that the E_3d_3 mudstone samples are in the main stage of hydrocarbon generation and could have good hydrocarbon generation capacity (Fig. 7c). Additionally, the geochemical parameters HI and GPI in the E_3d_3 mudstone samples gradually decreased with the increase of maturity (% R_o and %R_c) (Fig. 7d, e), and the PI exhibited a weak positive correlation with vitrinite reflectance (Fig. 7f). Indicating that the hydrocarbon generation rate of source rocks continuously strengthens from low mature to the mature stage, while the hydrocarbon generation potential gradually diminishes.

4.2. The difference in hydrocarbon generation rate based on Rock-Eval

The comparison of the hydrocarbon generation rate and transformation ratio of the investigated samples at different heating rates using Rock-Eval 6 is shown in Fig. 8 and Table 2. In the study, the FID signal was converted into an electrical signal value, and the hydrocarbon generation rate was quantitatively analyzed based on the electrical signal value. This approach can further characterize the variation in the hydrocarbon generation amount per unit time of OM. The heating rate has an impact on the pyrolysis of OM and the yield of hydrocarbon [62]. In the same sample, as the heating rate increased, the hydrocarbon generation rate of OM was significantly enhanced (Fig. 8 a1-f1). For example, when the heating rate of sample N2–6 increased from 10 ℃/min to 50 ℃/min, the maximum hydrocarbon generation rate (GR_{max}) of OM increased from 0.07 × 10^{-3} mg/g·s^{-1} to 0.32 × 10^{-3} mg/g·s^{-1} (Table 3). Additionally, the generation rate curves of some samples (N7–5, H18–1, SF1–2, ZC1–1) exhibited a bimodal distribution, indicating the characteristics of two stages of hydrocarbon generation. Meanwhile, the amplitude of the early hydrocarbon generation rate was more prominent at 50 ℃/min compared with 10 ℃/min, demonstrating that a higher heating rate is more effective in promoting the early generation of hydrocarbon from OM (Fig. 8 b1, d1-f1). Taking the heating rate of 50 ℃/min as an example, the GR_{50max} of the E_3d_3 mudstones and the mixed sample was (0.32–3.76)× 10^{-3} mg/g·s^{-1}, which was significantly smaller than the GR_{50max} of the modern organisms [(8.33–15.16)× 10^{-3} mg/g·s^{-1}]. However, the temperature corresponding to the maximum hydrocarbon generation rate ($T_{GR50max}$) of the E_3d_3 mudstones and the mixed sample is 389 ℃− 400 ℃, which is higher than the $T_{GR50max}$ of modern organisms (290 ℃−332 ℃),

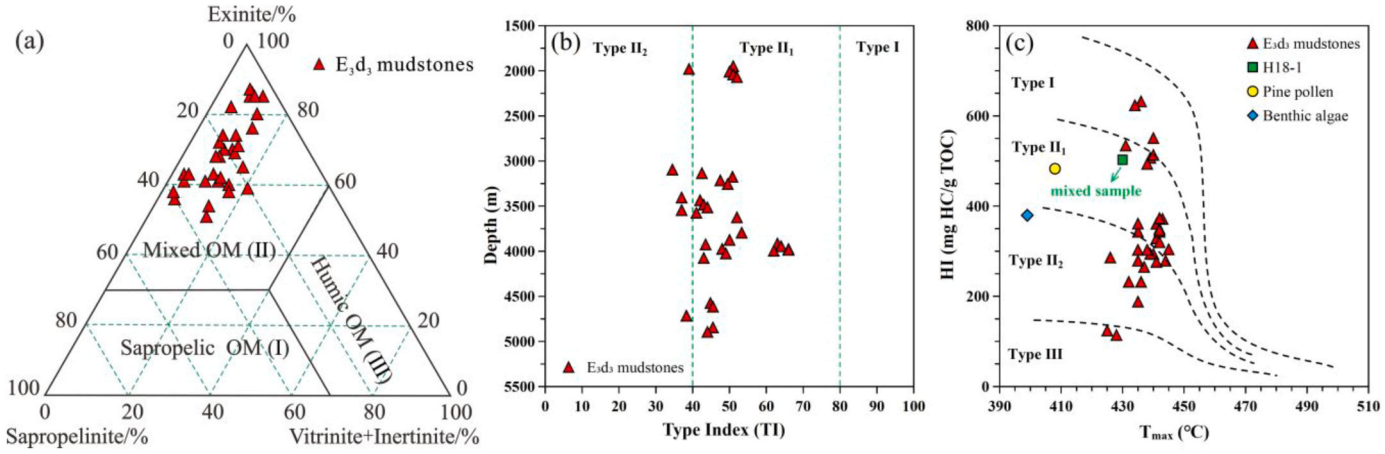

Fig. 6. The evaluation of OM types in the studied samples. (a) Maceral ternary diagram; (b) The distribution relationship between type index and depth; (c) The relationship between HI and T_{max}.

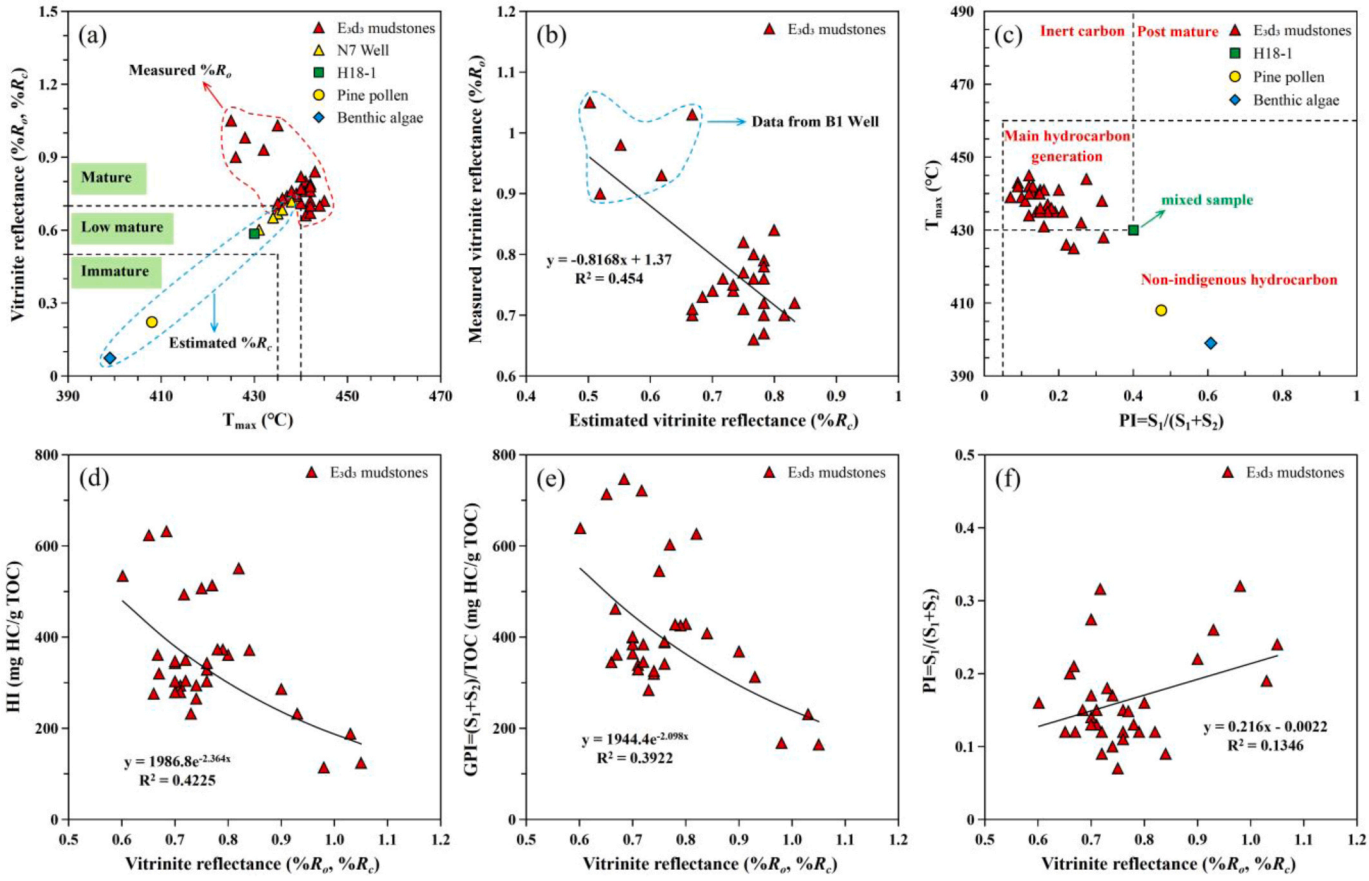

Fig. 7. (a) Relationship between vitrinite reflectance and T_{max}; (b) The correlation of vitrinite reflectance between measured value (%R_o) and estimated value (%R_c); (c) Cross plot of PI and T_{max} (according to [58]); Relationship between vitrinite reflectance and HI (d), GPI (e), PI (f) in the E_3d_3 mudstone samples.

suggesting that modern organisms are more prone to generate large amounts of hydrocarbons at the low mature stage.

Following the analysis, a good positive correlation was observed between GR_{50max} and TOC (Fig. 9a, R^2 =0.9922), while GR_{50max} remarkably decreased with the increase of T_{max} (Fig. 9b, R^2 =0.7249). This indicates that the hydrocarbon generation rate is closely related to the abundance and thermal maturity of OM, and the OM with high TOC and low maturity exhibits a greater hydrocarbon generation rate. Moreover, the higher hydrocarbon generation rates in modern organisms may be attributed to their lack of diagenetic alteration and rich biomass content. Previous studies have shown the presence of oil bodies in pine pollen grains, which contain a high stearic acid (54.7%) [42]. Similarly, benthic alga (laver) also contains a certain amount of lipids (1.96%) and proteins (32.16%) [43]. These biochemical components establish a solid foundation for hydrocarbon generation in modern organisms. As shown in Table 1, the S_1 (128.13 mg/g and 81.24 mg/g) and PI (0.47 and 0.61) of pine pollen and benthic algae were relatively high, indicating that they possess higher levels of free hydrocarbons at the low mature stage, which also further contributed to enhance the overall hydrocarbon generation rates.

The transformation ratios of the studied sample gradually increased with the rise of heating temperature, but the slope curves were different (Fig. 8 a2-f2). Generally, researchers consider that the OM reaches the threshold of hydrocarbon generation when the transformation ratio is 10%. The corresponding temperature span between 10% and 90% is typically regarded as the effective hydrocarbon generation range [16, 63]. Furthermore, the hydrocarbon generation process can be divided into three phases based on the transformation ratios: early generation (10%–25%), main generation (25%–65%), and late generation (65%–90%) [64]. The reaction temperatures corresponding to the transformation ratios at different generation phases of the six samples are displayed in Table 2. Overall, the higher the heating rate when increasing from 10 ℃/min to 50 ℃/min, the higher the reaction temperature required to achieve the same transformation ratio (Fig. 8 a2-f2). In the case of N4–11, to achieve a TR of 65% for OM, a temperature rise of 368 ℃ is required at a heating rate of 10 ℃/min, compared to 391 ℃ when using a heating rate of 50 ℃/min, resulting in a relative temperature increase of 23 ℃ (Fig. 8 c2). In contrast, the temperature range for initial hydrocarbon generation (TR=10%) temperature in modern organisms is 220 ℃– 250 ℃, which is lower than the temperature range observed in the E_3d_3 mudstones and mixed sample (250 ℃–315 ℃). However, the temperature range of the effective hydrocarbon generation interval (TR=10%–90%) for the modern organisms (155 ℃–165 ℃) is greater than that of the E_3d_3 mudstones and mixed sample (83 ℃–145 ℃) (Table 2). This illustrates that modern organisms have an excellent capacity for sustainable hydrocarbon generation. It is noteworthy that the temperature span of the modern organisms (25 ℃–39 ℃) in the early generation phase (TR=10%–25%) is lower than that of the E_3d_3 mudstones (35 ℃–50 ℃). In contrast, the temperature range for modern organisms in the late generation phase (TR=65%–90%) is approximately twice that of the other samples (Table 2). This suggests that modern organisms exhibit rapid hydrocarbon generation during the early phase and slower hydrocarbon generation in the late phase.

4.3. Comparison of kinetics characteristics

The laboratory can rapidly determine the thermal evolution and hydrocarbon generation process of OM based on the principle of temperature and time compensation [16]. By comparing the hydrocarbon

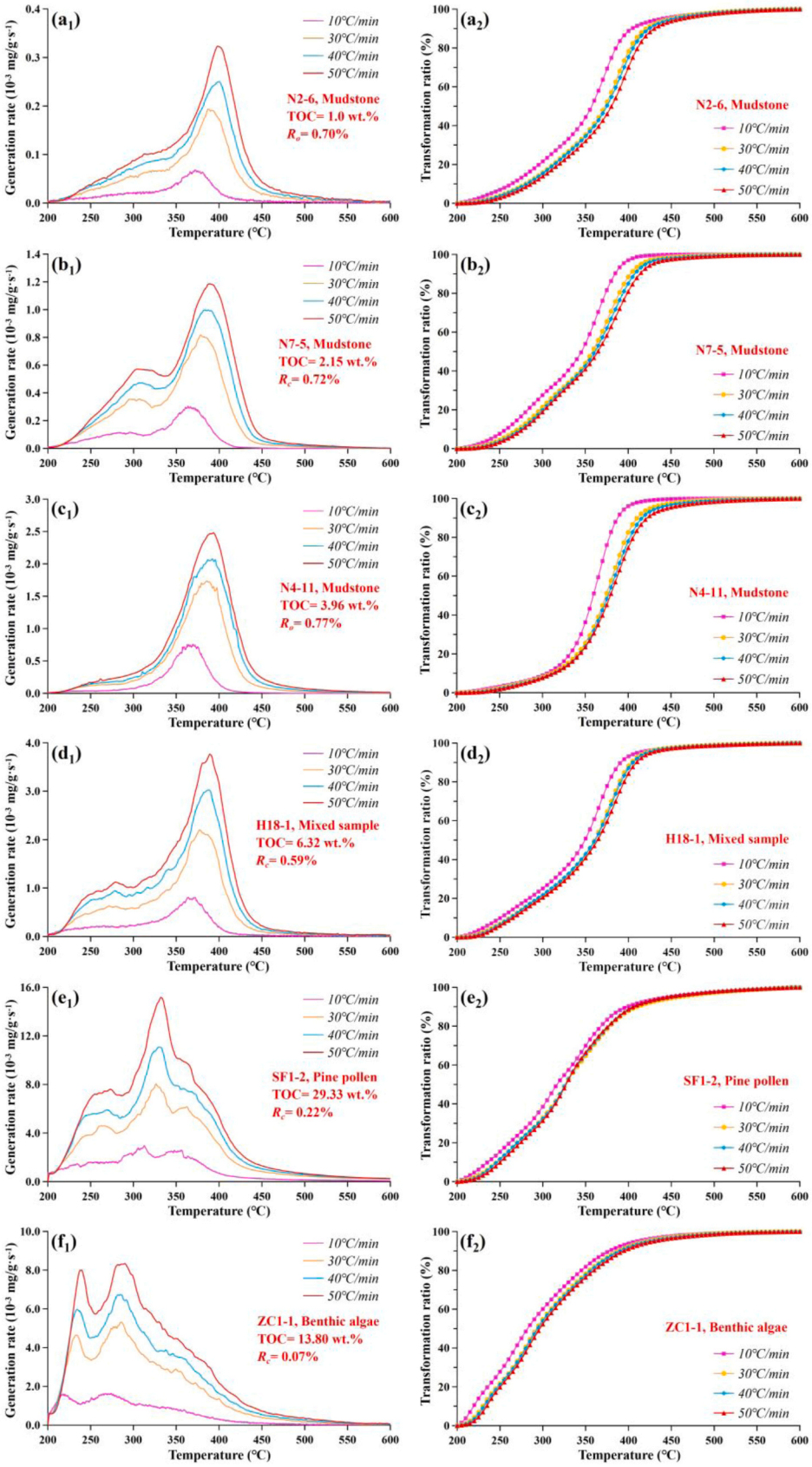

Fig. 8. The relationship of temperature with the hydrocarbon generation rate and the transformation ratio at different heating rates (10, 30, 40, 50 ℃/min). It shows that with the increase in heating rate, the hydrocarbon generation rate of OM is gradually enhanced, and the reaction temperature required to achieve the same transformation ratio is higher.

Table 2
The characteristics of hydrocarbon generation rate and the comparison of the corresponding temperature of transformation ratios from the investigated samples at different heating rates.

Samples	Heating rate (℃/min)	GR_{max} (10^{-3} mg/g·s^{-1})	T_{GRmax} (℃)	Fixed transformation ratios (TR, %) corresponding to temperature (℃)							
				TR= 10	TR= 25	TR= 65	TR= 90	TR span 10-25	TR span 25-65	TR span 65-90	TR span 10-90
N2-6	10	0.07	372	264	310	371	405	46	61	34	141
	30	0.19	387	280	325	387	420	45	62	33	140
	40	0.25	399	281	327	390	425	46	63	35	144
	50	0.32	400	286	332	395	430	46	63	35	144
N7-5	10	0.30	363	260	295	360	385	35	65	25	125
	30	0.82	378	270	310	375	405	40	65	30	135
	40	1.00	387	275	311	378	410	36	67	32	135
	50	1.18	389	280	315	383	415	35	68	32	135
N4-11	10	0.76	369	305	340	368	388	35	28	20	83
	30	1.74	386	310	349	385	410	39	36	25	100
	40	2.08	392	315	351	389	415	36	38	26	100
	50	2.48	394	315	352	391	422	37	39	31	107
H18-1	10	0.81	364	250	300	364	391	50	64	27	141
	30	2.20	377	261	310	375	404	49	65	29	143
	40	3.02	387	262	310	377	405	48	67	28	143
	50	3.76	389	265	314	380	410	49	66	30	145
SF1-2	10	2.94	313	235	274	342	400	39	68	58	165
	30	8.04	326	245	282	350	410	37	68	60	165
	40	11.08	329	246	283	349	405	37	66	56	159
	50	15.16	332	250	286	348	405	36	62	57	155
ZC1-1	10	1.63	274	220	245	310	378	25	65	68	158
	30	5.31	285	230	256	320	389	26	64	69	159
	40	6.73	285	232	259	321	390	27	62	69	158
	50	8.33	290	235	260	323	394	25	63	71	159

Table 3
The weighted average values of the activation energy from the investigated samples obtained by the SFFP and MFFP models, respectively.

Samples	Sample types	GR_{50max} (10^{-3} mg/g·s^{-1})	E_{ave} (KJ/mol)	A_s (s^{-1})	ln (A_s)	E_{mean} (KJ/mol)
N2-6	mudstone	0.32	219.35	2.25×10^{16}	37.65	236.61
N7-5	mudstone	1.18	221.57	9.91×10^{16}	39.14	223.05
N4-11	mudstone	2.48	239.84	7.69×10^{17}	41.18	276.96
H18-1	mixed sample	3.76	312.79	4.49×10^{24}	56.76	326.72
SF1-2	pine pollen	15.16	389.26	1.98×10^{32}	74.36	385.69
ZC1-1	benthic algae	8.33	221.11	3.86×10^{15}	42.70	296.39

E_{ave} and A_s are the weighted average of activation energy and frequency factor obtained in the SFFP model. E_{mean} is the weighted mean of activation energy obtained in the MFFP model.

generation curves of modern organisms and source rock samples subjected to different heating rates, and employing kinetic software to fit the optimal hydrocarbon generation path. The single-frequency factor model (SFFP model) and multi-frequency factor model (MFFP model) in parallel first-order reactions were used to analyze the kinetic characteristics [18,21]. The comparison of the activation energy (E_a) and frequency factor (A) obtained using two models is shown in Fig. 10, Table 3, and Table 4.

The weighted average activation energy (E_{ave}) and frequency factor (A_s) of the E_3d_3 mudstones and the mixed sample in the SFFP model are 219.35–312.79 KJ/mol and 2.25×10^{16}-4.49×10^{24} s^{-1}, respectively (Fig. 10 a1-d1, Table 3). However, E_{ave} and A_s of pine pollen and benthic algae samples are 389.26 KJ/mol, 221.11 KJ/mol, 1.98×10^{32} s^{-1}, and 3.52×10^{18} s^{-1}, respectively (Fig. 10 e1-f1, Table 3). This indicates that the kinetic parameters of terrestrial plants and aquatic algae are different, and the threshold of hydrocarbon generation from algae is lower. The weighted mean activation energy (E_{mean}) of the studied samples in the MFFP model is between 223.05 and 385.69 KJ/mol, which is similar to the results of the SFFP model, whereas the activation energy range of the MFFP model is wider (Fig. 10 a2-f2, Table 3). The activation energy (E_{a-m}) and the frequency factor ln(A_m) in the MFFP model do not strictly follow a positive correlation, as evidenced by the cases of N4–11, H18–1, and SF1–2 samples. In these instances, when the activation energy exceeds 450 KJ/mol, the corresponding frequency factor becomes significantly smaller (Fig. 10 c2-e2). However, E_{ave} and ln(A_s) of the studied samples present a strong positive correlation in the SFFP model (Fig. 11a, R^2 =0.9814), indicating that a single frequency factor has certain limitations and does not fully respond to some of the variations in the evolution of hydrocarbons.

The analysis of activation energy (E_{a-m}) and frequency factor (A_m) corresponding to different transformation ratios (TR) in the MFFP model is presented in Table 4. It is evident that for the majority of samples, both E_{a-m} and A_m show a gradual increase as TR rises within the effective hydrocarbon generation interval (TR=10%−90%). However, this trend is not consistently followed, as exemplified by the N4–11 sample with an A_m value of only − 2.51×10^{10} s^{-1} in the TR= 10%− 90% span. The E_{a-m} of the investigated samples exhibits a wide distribution range (56.47–372.77 KJ/mol) within the TR= 10%− 90% span (Table 4). There is a greater variation in the spanning range of E_{a-m} in the three phases of early generation (TR=10%−25%), major generation (TR=25%−65%), and late generation (TR=65%−90%) (Fig. 11b, Table 4). It indicates that the chemical structure of OM in modern organisms and mudstone samples is more non-homogeneous, and the hydrocarbon generation evolution is intricate. Therefore, the application of the MFFP model could better characterize the variation of kinetic parameters in different hydrocarbon generation stages. Comprehensive analysis suggests that the activation energy obtained by the SFFP model has a narrow distribution range. Whereas, the weighted average activation energy in the MFFP model is similar to that in the SFFP model, and the distribution range of the activation energy is more extensive. Previous studies argued that the SFFP model did not adequately account for the activation energy required for early and late phases of hydrocarbon generation, leading to a limited range of activation energy values. In contrast, the MFFP model places greater emphasis on the entire process of hydrocarbon generation evolution, aligning more closely with the actual geological process [21].

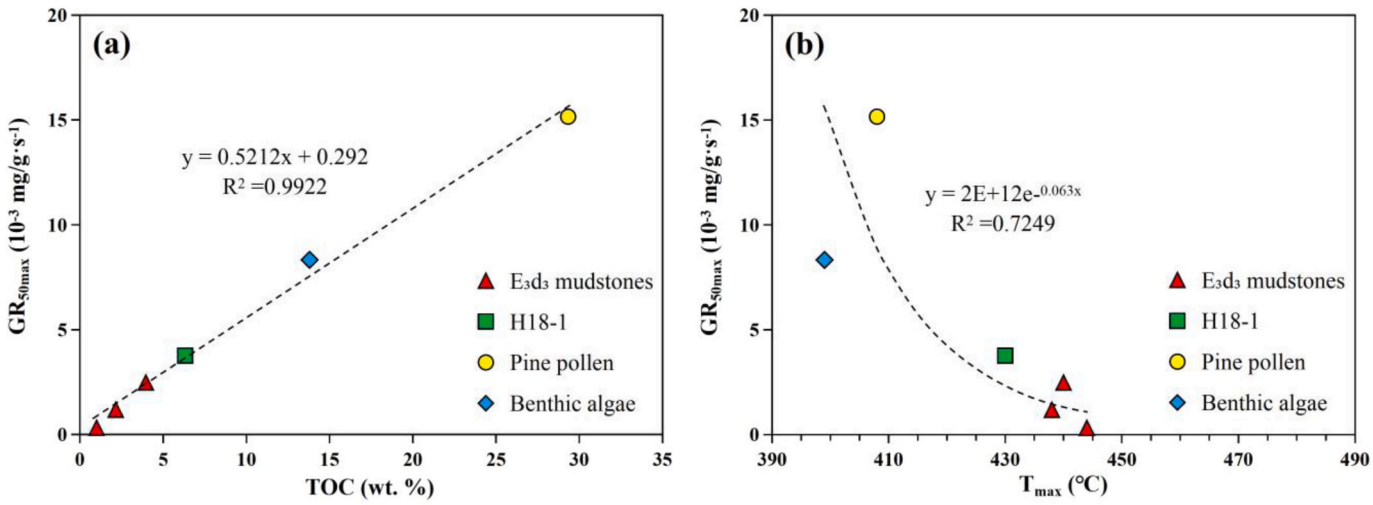

Fig. 9. Correlation analysis of the maximum hydrocarbon generation rate (GR_{50max}) with TOC (a) and T_{max} (b) at a heating rate of 50 ℃/min.

The Pearson correlation analysis of organic geochemical parameters with the kinetic parameters of the studied samples revealed two significant correlation trends between the two types of parameters (Fig. 12). Specifically, in the case of similar OM types, the higher the OM abundance and generation potential parameters (TOC, S_1, S_2, GP, and GPI, etc.), the greater the hydrocarbon generation rate (GR_{50max}), weighted average/mean activation energy (E_{ave} and E_{mean}) and frequency factor ln(A_s) of the samples. In contrast, the maturity parameters (R_o and T_{max}) displayed a certain negative correlation tendency with the kinetic parameters (Fig. 12). It illustrates that the kinetic characteristics of hydrocarbon generation reaction are greatly influenced by the quality parameters of OM, which further highlights the complexity of the hydrocarbon generation evolution process.

4.4. *Thermal simulation yield and product characteristics*

The hydrocarbon yield of the mixed sample (H18–1) under different temperature conditions can be obtained by employing a water-added closed thermal simulation experiment (Fig. 13a). As the simulated temperature increased, the pressure within the closed autoclave also increased, ranging from 2.3 MPa (200 ℃) to 22.3 MPa (450 ℃) (Table 5). This increase in pressure corresponds to a gradual rise in the conversion rate and the yield of hydrocarbon, indicating hydrocarbon generation plays an obvious role in pressurization. In the temperature stage of 200 ℃ to 320 ℃, the yield of hydrocarbon gas was very weak, less than 40 mg/g TOC, and it was mainly dominated by generating oil. Subsequently, as maturity increased, the yield of hydrocarbon gas gradually enhanced. At temperatures of 400 ℃ and 450 ℃, the yield reached 403.40 mg/g TOC and 414.76 mg/g TOC, respectively, tending to stabilize (Fig. 13a). The yield curve of generated oil displayed a pattern of increasing and then decreasing, indicating a substantial conversion of kerogen into oil during low mature to mature stages. However, as maturation progressed beyond the high mature stage, the capacity for oil generation gradually diminished until it was ultimately exhausted [1].

It is noteworthy that the H18–1 sample has two yield peaks in the process of oil generation (Fig. 13a). The temperature of the first peak is 300 ℃ with an oil yield of 572.06 mg/g TOC, and the temperature of the second peak is 370 ℃ with an oil yield of 470.12 mg/g TOC (Fig. 13a). This suggests that there are two stages of oil generation evolution in the mixed sample. In contrast, the hydrocarbon generation rate curves of the sample (N4–11) without organism components in the pyrolysis process exhibited a single-peak distribution, with peak temperatures ranging from 369 ℃ to 394 ℃ at different heating rates, and the generation rate at the low mature stage was small (Fig. 8c1, Table 2). Previous studies have proven that the evolution of OM within the Dongying Formation source rocks follows a hydrocarbon generation model characterized by a bimodal pattern. This is evident in the relationship between the S_1/TOC and the chloroform asphalt "A"/TOC, which varies in accordance with burial depth or maturity. Simultaneously, it is considered that the two components of benthic algae amorphous and Pinaceae sporopollen contribute significantly to the hydrocarbon generation of source rocks at the low-mature and mature stages [37]. The target sample (H18–1) for the thermal simulation was mixed with modern benthic algae (wt.5%) and pine pollen (wt.5%). The results showed that the yield characteristics of the generated oil were consistent with the bimodal hydrocarbon generation model, further confirming the substantial hydrocarbon generation capacity of these two particular components within the source rocks of the Dongying Formation. Previous studies have comprehensively elucidated the hydrocarbon generation mechanism of pine pollen. These studies indicated that when the simulated temperature was below 260 ℃, the inner protoplasm (lipids) of pine pollen contributed to the generation of early immature to low-mature oil. When the temperature reaches 260 ℃– 400 ℃, the sporopollenin in the extine of pine pollen becomes the predominant hydrocarbon-generating precursor, yielding light oils [5,6]. In contrast, benthic algae are abundant in S, O, N, and other heteroatoms and generally exhibit low activation energy (averaging 220 KJ/mol), allowing them to generate numerous hydrocarbons during immature to low-mature stages [9,11]. Simultaneously, the hydrocarbon generation potential of benthic algae was comparable to type II kerogen, and it also demonstrated a considerable hydrocarbon yield during the mature stage [10,12]. Therefore, pine pollen and benthic algae have a wide range of activation energies and hydrocarbon windows throughout the effective hydrocarbon production period. The activation energies of SF1–2 and ZC1–1 samples in the MFFP model have a wide distribution range, which also strongly supports this view (Fig. 10 e2, f2). The characteristics of the total generated hydrocarbon yield curve are similar to the generated oil yield, and the two peaks of the total hydrocarbon yield at 300 ℃ and 370 ℃ are 584.46 mg/g TOC and 740.44 mg/g TOC, respectively, revealing a good hydrocarbon generation capacity (Fig. 13a).

Under different temperature conditions, the generated liquid hydrocarbons exhibited varying colors after being dissolved in the dichloromethane reagent. As the thermal simulation temperature increased, the color of the generated liquid hydrocarbons gradually changed from gray-green to dark brown to light yellow, signifying that the properties of the generated liquid hydrocarbons at different stages of maturity were discriminative (Fig. 13b). The content of saturated hydrocarbons, aromatic hydrocarbons, heterocompounds and asphaltenes in the composition of the generated oil was 18.06%– 36.64%,

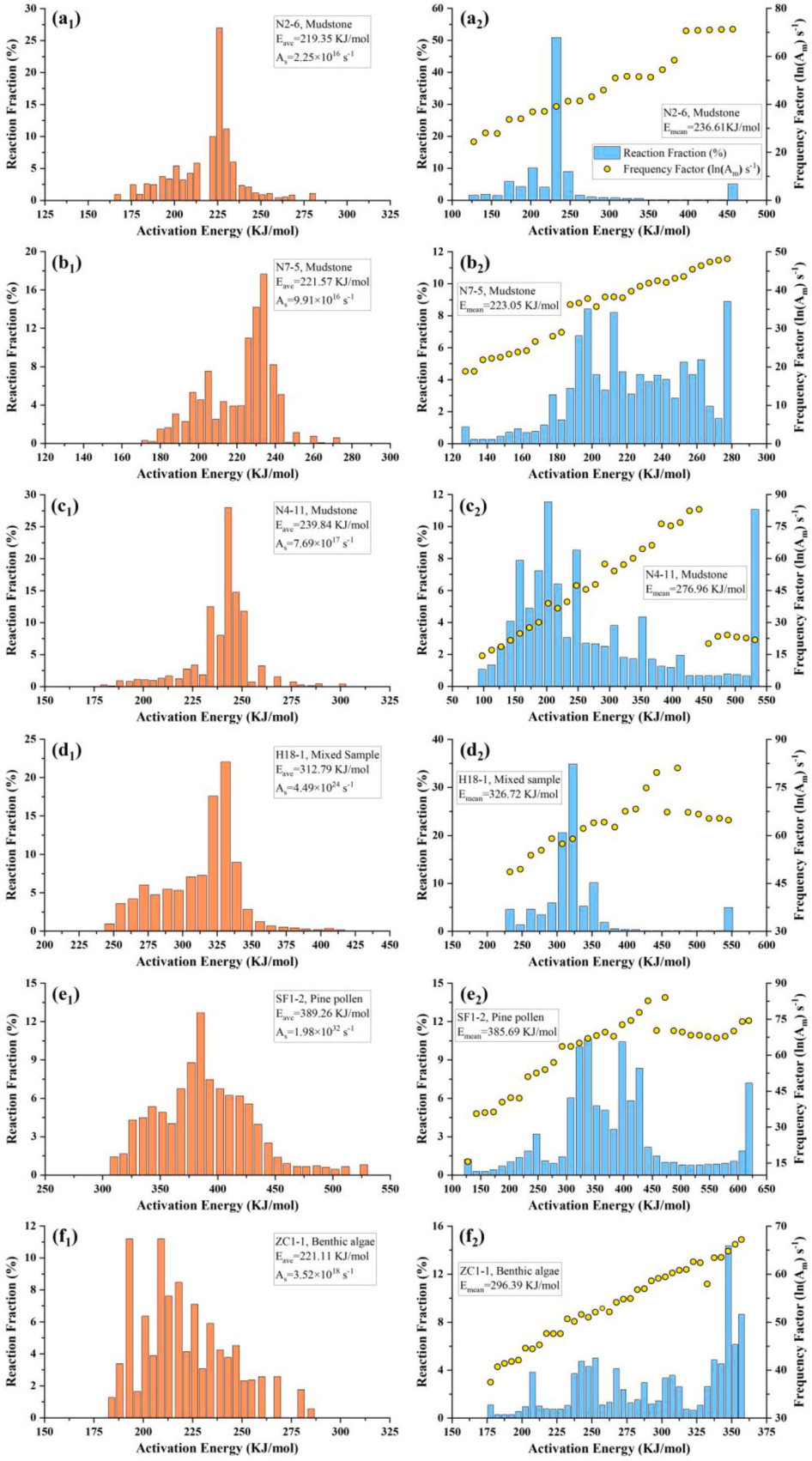

Fig. 10. The reaction fraction of activation energy in SFFP mode (a1-f1) and the distribution characteristics of activation energy and frequency factor $\ln(A_m)$ obtained in MFFP mode (a2-f2) from the investigated samples.

Table 4
The distribution of activation energy (E_{a-m}) and frequency factor (A_m) corresponding to different transformation ratios (TR) in the MFFP model.

Samples		Fixed transformation ratios (TR) corresponding to activation energy (E_{a-m}) and frequency factor (A_m)				
		TR= 10%	TR= 25%	TR= 65%	TR= 90%	TR span 10%−90%
N2-6	E_{a-m} (KJ/mol)	178.39	210.07	235.69	264.71	86.32
	A_m (s^{-1})	2.21×10^{15}	9.26×10^{15}	3.73×10^{16}	1.71×10^{18}	1.70×10^{18}
N7-5	E_{a-m} (KJ/mol)	180.93	196.95	238.48	271.66	90.73
	A_m (s^{-1})	2.47×10^{12}	3.53×10^{16}	4.57×10^{17}	2.68×10^{20}	2.68×10^{20}
N4-11	E_{a-m} (KJ/mol)	155.46	185.29	293.84	528.23	372.77
	A_m (s^{-1})	2.96×10^{10}	1.20×10^{13}	1.02×10^{22}	4.51×10^{9}	-2.51×10^{10}
H18-1	E_{a-m} (KJ/mol)	267.59	304.6	324.73	358.21	90.62
	A_m (s^{-1})	3.49×10^{23}	1.85×10^{22}	2.73×10^{24}	1.86×10^{28}	1.86×10^{28}
SF1-2	E_{a-m} (KJ/mol)	250.9	323.13	404.84	587.63	336.73
	A_m (s^{-1})	1.64×10^{23}	1.51×10^{22}	1.96×10^{30}	3.66×10^{29}	3.66×10^{29}
ZC1-1	E_{a-m} (KJ/mol)	225.88	250.35	338.68	353.63	127.75
	A_m (s^{-1})	4.73×10^{20}	3.48×10^{22}	4.35×10^{23}	3.17×10^{29}	3.17×10^{29}

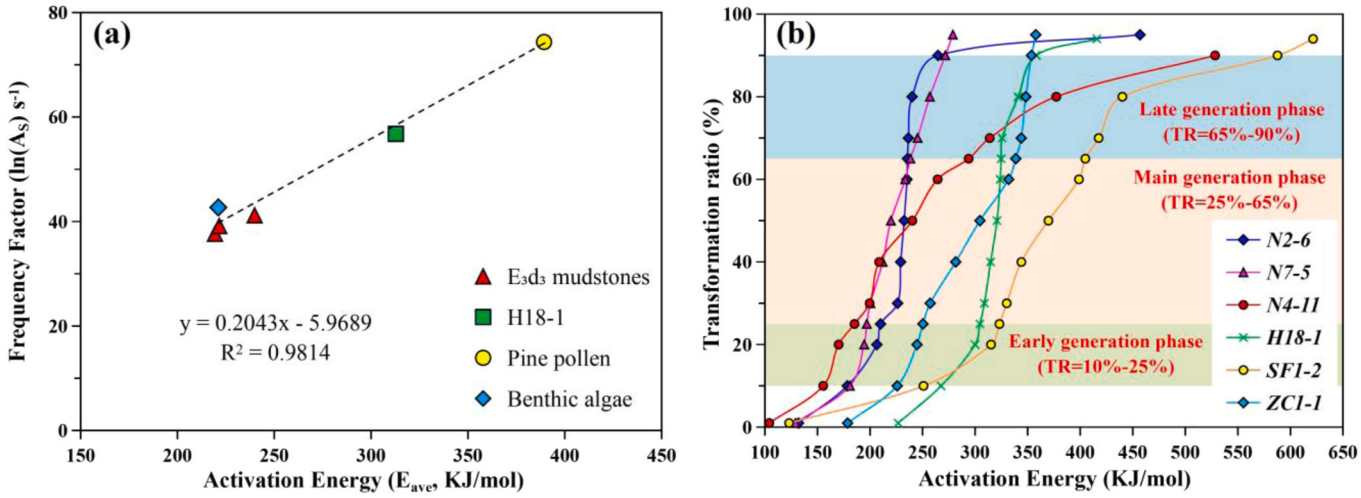

Fig. 11. (a) Correlation between the weighted average activation energy (E_{ave}) and ln(A_s) in the SFFP model; (b) The relationship between the activation energy and the transformation ratios of the studied sample in the MFFP model, where the generation phase is divided from ref. [64].

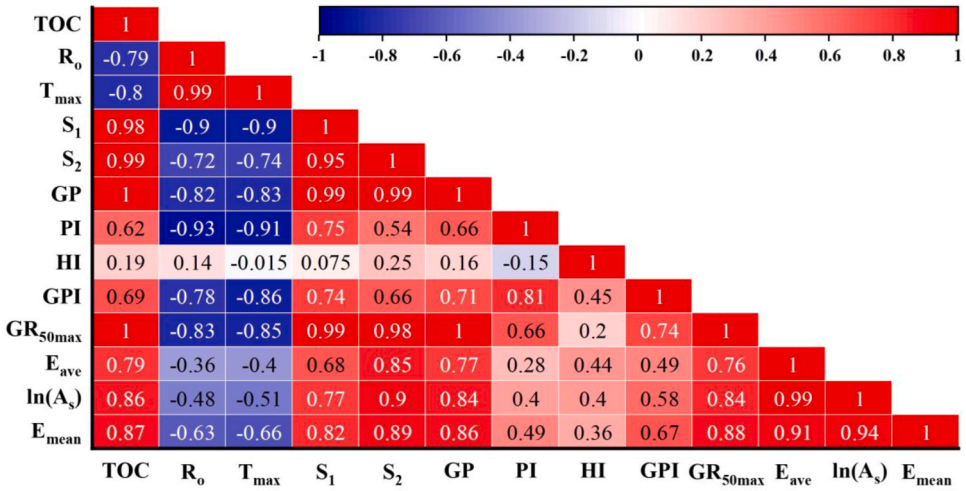

Fig. 12. The Pearson correlation matrix analysis of organic geochemical parameters and the kinetic parameters of the study samples. Abbreviations of parameters are interpreted in Tables 1, 2, and 3.

14.81%− 26.37%, 24.54%− 38.88%, and 12.96%− 33.81%, respectively (Table 5). The variations in the content of each component concerning the simulated temperature did not exhibit an apparent regularity (Fig. 13c). Particularly, the relative content of saturated hydrocarbons and heterocompounds in the generated oil at 450 ℃ was the minimum (18.06%) and the maximum (38.88%), respectively. This observation contradicts the theoretical expectations regarding the evolution of crude oil components. One potential explanation is that the saturated hydrocarbon components of liquid hydrocarbons are more likely to undergo cracking into gaseous hydrocarbons in the closed

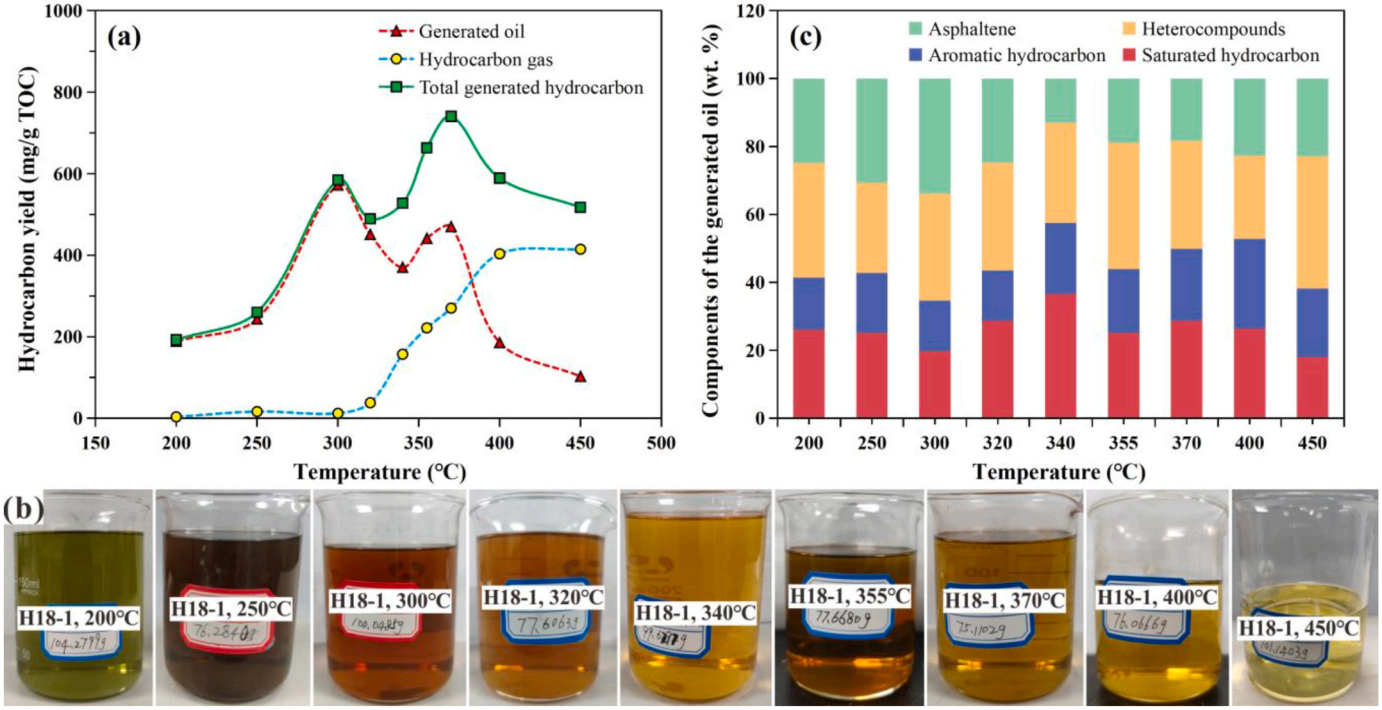

Fig. 13. (a) The relationship between hydrocarbon yield and temperature variations in the enclosed thermal simulation experiment; (b) The physical phenomena of the generated oil at different temperatures; (c)The distribution characteristics of the generated oil components.

Table 5
Hydrocarbon yield and generated oil composition properties of the mixed sample (H18–1) at different simulated temperatures under closed autoclave conditions.

Simulated temperature (℃)	Autoclave pressure (MPa)	Hydrocarbon yield (mg/g TOC)			Components of the generated oil (wt%)			
		Generated oil	Hydrocarbon gas	Total generated hydrocarbon	Saturated hydrocarbon	Aromatic hydrocarbon	Heterocompounds	Asphaltene
200	2.3	189.05	3.57	192.62	26.06	15.30	33.71	24.93
250	4.5	243.52	16.65	260.17	25.14	17.60	26.54	30.72
300	6.7	572.06	12.40	584.46	19.77	14.90	31.52	33.81
320	8.4	451.02	38.17	489.19	28.71	14.81	31.67	24.81
340	9.6	370.28	157.22	527.50	36.64	20.85	29.55	12.96
355	11.9	441.44	221.89	663.34	25.17	18.71	37.19	18.93
370	13.8	470.12	270.31	740.44	28.63	21.28	31.74	18.35
400	15.4	185.60	403.40	589.00	26.37	26.37	24.54	22.72
450	22.3	102.86	414.76	517.62	18.06	20.14	38.88	22.92

environment at the high maturity stage, thereby reducing the relative content.

4.5. Geological implication

The burial and hydrocarbon generation histories of the E_3d_3 interval of the Dongying Formation were obtained from the simulation analysis of wells N2, N7, and N4 in the Bozhong area utilizing PetroMod software based on the geostructural, geochemical, and MFFP model kinetic parameters (Figs. 14 and 15). The burial history data displays that the Bozhong area experienced uplift during the late Oligocene period, leading to different degrees of erosion in the upper sedimentary layers of the Dongying Formation. Specifically, the N7 well located in the southwestern of the study area, significantly suffered from this uplift and erosion (Fig. 14b). These findings align with previous research [46]. This study further reconstructed the thermal maturity history, transformation ratios, and hydrocarbon generation rate to estimate the hydrocarbon generating capacity of the E_3d_3 mudstones interval. The temperature and maturity simulation results from different wells reveal that the E_3d_3 mudstones are overall in a low mature-mature stage. The current temperature in the N2 and N4 wells is 133.8 ℃ and 122.2 ℃, respectively, with maturity levels of 0.81% and 0.76%R_o (Fig. 14a, c). However, the current temperature in the N7 well is only 94.3 ℃ due to uplift and erosion, resulting in a lower maturity (0.58%R_o) (Fig. 14b). The simulation results depicted in Fig. 15 show that wells N7 and N4 entered into the early generation stage at around 29.7 Ma, and the hydrocarbon generation rate increased rapidly, with both wells reaching their initial peak generation rate (0.069 and 0.057mgHC/gTOC/Ma) at approximately 28.4 Ma and 27.4 Ma, respectively. This suggests that the early stages of hydrocarbon generation were quite pronounced during this time. At present, wells N7 and N4 are in the main generation phase, with 55.01% and 62.23% transformation ratios, respectively, yet the hydrocarbon generation rates are not high and this might have been affected by the lower degree of thermal evolution of the OM. Furthermore, the activation energy and frequency factor data obtained from the mixed sample (H18–1) under the MFFP model were also applied to well N4 to simulate hydrocarbon generation. The results indicate that H18–1 also undergoes two phases of hydrocarbon generation, but the transformation ratio and hydrocarbon generation rate are significantly lower than those observed in well N4 (Fig. 15). This discrepancy be attributed

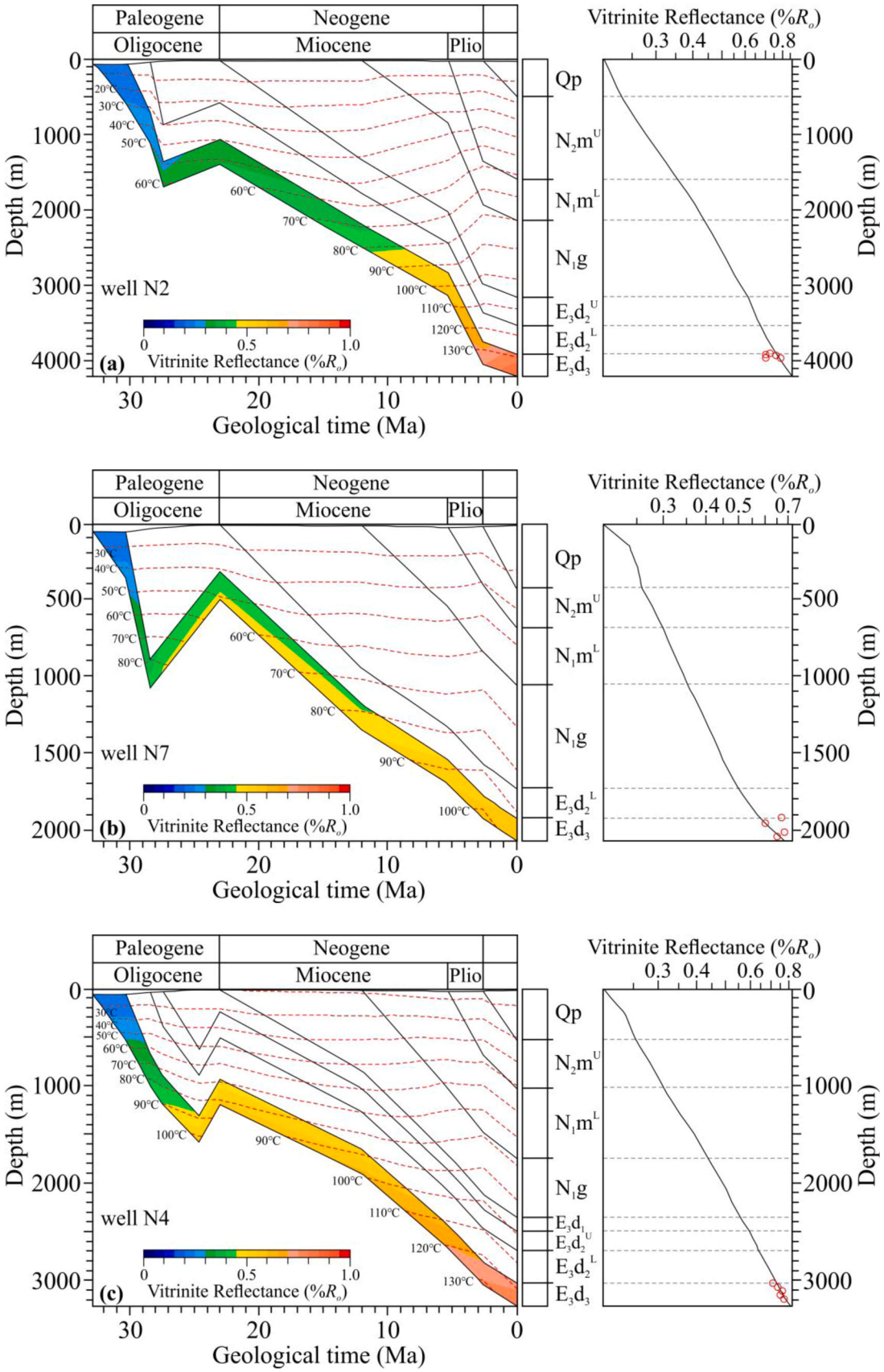

Fig. 14. Burial history and thermal history of the E_3d_3 source rocks in the Bozhong Sag, (a) well N2, (b) well N7, and (c) well N4.

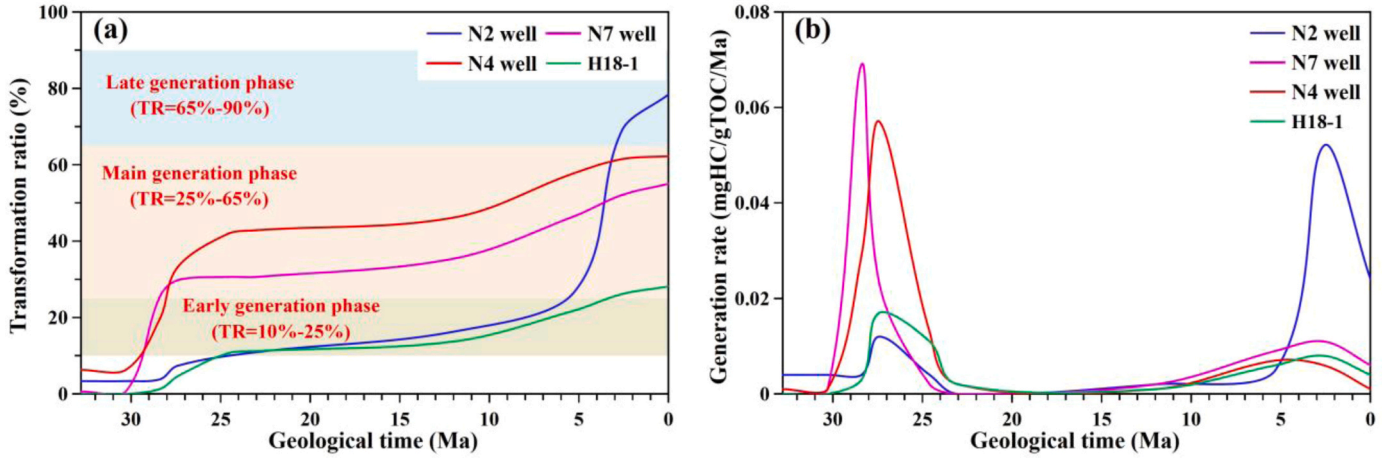

Fig. 15. The distribution characteristics of transformation ratios and generation rates in wells N2, N7, and N4 during geological time. Showing there are two periods of hydrocarbon generation in the E_3d_3 mudstones.

to the lower maturity of H18–1. Nevertheless, the evolutionary pattern of two-phase hydrocarbon generation in both modern organisms remains reliable.

In contrast, the N2 well exhibits different results in the evolution of hydrocarbon generation. It entered the early generation phase at about 25.4 Ma, and the hydrocarbon generation rate was relatively small in the low mature stage (peak value of 0.012mgHC/gTOC/Ma). The transformation ratio and generation rate increased rapidly after 5.3 Ma, reaching a peak generation rate of 0.052mgHC/gTOC/Ma in the mature stage at 2.6 Ma. Currently, the simulated transformation ratio is 78.42% and is entering the late generation phase. The well experienced rapid hydrocarbon generation during the main generation phase, resulting in a short duration (Fig. 15). However, the measured R_o of the source rock in well N2 is 0.70%– 0.78% (Table 1), which is inconsistent with the current higher transformation ratio. Investigation of the burial history of well N2 reveals that the strata of the Dongying Formation underwent a rapid subsidence phase during the Pliocene (5.3–2.6 Ma), and its strata temperature rose rapidly to above 130 ℃. Furthermore, well N2 is located in the northern Bozhong sag, adjacent to the Shijiutuo uplift. Previous studies have shown that this area has a high heat flow value (70–80 mW/m^2) in the Neogene [41,51]. The high heat flow and rapid subsidence may have contributed to the rapid hydrocarbon generation of the OM in a short period, consequently leading to an increase in the transformation ratios (Fig. 15a).

Comprehensive basin simulation analysis suggests two distinct periods of hydrocarbon formation within the mudstone interval of the Dongying Formation. The first occurred during the Oligocene (approximately 29.7–23.1 Ma), while the second took place in the Pliocene (5.3 Ma to present). This discovery aligns with the generation rate findings derived from pyrolysis and autoclave simulation (Fig. 8 and Fig. 13). Moreover, the OM abundance within the E_3d_3 interval is high and the predominant OM types are II_1 and II_2, and these source rocks are primarily in the main generation phase. The kinetic characteristics of modern organisms further demonstrate that benthic algae amorphous and Pinaceae sporopollen play a crucial role in both stages of hydrocarbon generation. Furthermore, the sand layers and sublacustrine fan sand bodies within the thick mudstone of the Dongying Formation in the Bozhong Sag are relatively well-developed, which creates favorable conditions for hydrocarbon accumulation either near-source or intra-source [31,37,65]. Consequently, Bozhong Sag near the source kitchen of the Dongying Formation offers promising prospects for oil and gas exploration.

5. Conclusions

(1) The modern organisms (pine pollen and benthic algae) are characterized by high TOC, high GP, and immaturity, and the OM type is consistent with the E_3d_3 mudstones (mainly type II_1-II_2), both of them possessing excellent oil generation potential. The comparison of generation rates and transformation ratios in Rock-Eval pyrolysis shows that a higher heating rate is preferable to promote early hydrocarbon generation and the OM with high TOC and low maturity exhibits a greater hydrocarbon generation rate.

(2) The SFFP model employs a single frequency factor, which has certain limitations and tends to disregard the activation energy required for both the early and late generation stages, leading to a narrow distribution range of activation energy. The MFFP model focuses more on the kinetic reactions occurring throughout all generation stages, resulting in a wider range of activation energy values that align more closely with the actual geological process. The distribution of activation energy is closely related to the OM quality parameters. Compared with the E_3d_3 interval mudstone, modern organisms exhibit broad activation energy spans and excellent sustained hydrocarbon generation capabilities.

(3) The water-added enclosed thermal simulation demonstrates that there are two peak yields in the process of oil generation from the mixed sample, the first peak is at 300 ℃ (oil yield 572.06 mg/g TOC) and the second peak is 370 ℃ (oil yield 470.12 mg/g TOC). Similar results are obtained from basin simulation analysis and it is concluded that the Dongying Formation mudstones have experienced two phases of hydrocarbon generation in the Oligocene (about 29.7–23.1 Ma) and the Pliocene (5.3 Ma to present), and are currently in the main generation phase. The kinetic characteristics of modern organisms highlight the pivotal role played by the abundant benthic algal amorphous and Pinaceae sporopollen components in the two hydrocarbon generation stages.

(4) A comprehensive analysis of kinetics, thermal simulation, and basin modeling suggests that although theoretically modern organisms have not experienced diagenesis in geological processes, the presentation of hydrocarbon generation characteristics may not be accurate. However, it is still worthwhile to attempt the analysis of the evolution trend and qualitative pattern of hydrocarbon generation in parent material components. In conclusion, the method of applying modern organisms analogy to characterize the hydrocarbon generation evolution of the dominant

components of lacustrine source rocks seems to be feasible for reference.

CRediT authorship contribution statement

Guoxiong Li: Conceptualization, Data curation, Investigation, Methodology, Software, Writing – original draft. **Chenglin Liu:** Conceptualization, Supervision, Validation, Writing – review & editing. **Rizwan Sarwar Awan:** Investigation, Validation, Writing – review & editing. **Xiaoyi Yang:** Data curation, Investigation, Methodology. **Dehao Feng:** Data curation, Investigation, Methodology. **Feilong Wang:** Resources. **Xiaoxiang Zeng:** Investigation, Methodology, Visualization. **Hong Yang:** Investigation, Methodology, Visualization. **Su Jiajia:** Investigation, Methodology. **Yuping Wu:** Investigation, Visualization. **Taozheng Yang:** Investigation, Methodology. **Zhen-gang Ding:** Investigation, Methodology. **Zhangxing Chen:** Supervision, Writing – review & editing.

Declaration of Competing Interest

The authors declare that they have no known competing financial interests or personal relationships that could have appeared to influence the work reported in this paper.

Data availability

Data will be made available on request.

Acknowledgements

This work is financially supported by the National Key R&D Program of China (Grant No. 2021YFA0719000) and the Major Research Program of the Tianjin Branch of CNOOC China Limited (CCL2020TJX0NST1266).

References

[1] B.P. Tissot, D.H. Welte, Petroleum Formation And Occurrence, Springer Science & Business Media, 1978.
[2] Z. Chen, G. Zhou, R. Alexander, A biomarker study of immature crude oils from the shengli oilfield, People's Republic of China, Chem. Geol. 113 (1994) 117–132.
[3] T. Wang, Immature oils in China and their genetic mechanisms, Acta Geol. Sin. Ed. 74 (2000) 632–640.
[4] D. Huang, Advances in hydrocarbon generation theory (i): generation and evolution model for immature oils and hydrocarbon, J. Pet. Sci. Eng. 22 (1999) 121–130.
[5] X. Jin, J. Song, H. Wei, H. Chen, Twice hydrocarbon-generating mechanism of sporopollen during thermopressurized simulation, Pet. Explor. Dev. 25 (1998) 10–14.
[6] L. Ji, Q. Meng, J. Zheng, W. Zhang, Y. Xu, S. Wang, Biomarker distributions of saturated hydrocarbons from remains extracts of thermal simulation of pine pollens, Acta Sedimentol. Sin. 17 (1999) 644–650.
[7] X. Jin, A comparison study on the hydrocarbon productivity of pollen and algae, Pet. Explor. Dev. 27 (2000) 28–32.
[8] L. Ji, Y. Zhu, Characteristic changes of pine pollen in thermal degradation experiments, Acta Micropalaeontol. Sin. 21 (2004) 412–418.
[9] Q.J. Jiang, Q. Wang, Q. Cheng, C. Zhang, W. Liu, Discussion on the kinetic characteristics of hydrocarbon generation of different maceral source rocks, Pet. Geol. Exp. 27 (2005) 512–518.
[10] Q. Meng, L. Ma, A. Zou, Z. Li, Comparison of characteristics of hydrocarbon generation for different alga, Pet. Geol. Exp. 30 (2008) 281–285.
[11] Q.G. Jiang, Y.B. Wang, J.Z. Qin, Kinetic study on hydrocarbon generation mechanism of modern organisms, Acta Sedimentol. Sin. 27 (2009) 546–550.
[12] J. Qin, B. Shen, X. Fu, G. Tao, G. Teng, Ultramicroscopic organic petrology and potential of hydrocarbon generation and expulsion of quality marine source rocks in South China, Oil Gas Geol. 31 (2010) 826–837.
[13] W. Obeid, E. Salmon, M.D. Lewan, P.G. Hatcher, Hydrous pyrolysis of scenedesmus algae and algaenan-like residue, Org. Geochem. 85 (2015) 89–101.
[14] S. Liu, G. Gao, W. Gang, B. Xiang, M. Wang, Differences in geochemistry and hydrocarbon generation of source-rock samples dominated by Telalginite and Lamalginite: a case study on the Permian Saline Lacustrine source rocks in the Jimusaer Sag, NW China, Pet. Sci. 20 (2023) 141–160.
[15] J. Teng, H. Deng, Y. Xia, W. Chen, M. Fu, Controls of amorphous organic matter on the hydrocarbon generation potential of lacustrine shales: a case study on the chang 7 member of Yanchang formation, Ordos Basin, North China, Energy Fuels 35 (2021) 5879–5888.
[16] A.S. Pepper, P.J. Corvi, Simple kinetic models of petroleum formation. Part i: oil and gas generation from Kerogen, Mar. Pet. Geol. 12 (1995) 291–319.
[17] V. Burklé-Vitzthum, R. Bounaceur, R. Michels, G. Scacchi, P. Marquaire, Kinetic parameters for the thermal cracking of simple hydrocarbons: from laboratory to geological time-temperature conditions, J. Anal. Appl. Pyrolysis 125 (2017) 40–49.
[18] V. Dieckmann, Modelling petroleum formation from heterogeneous source rocks: the influence of frequency factors on activation energy distribution and geological prediction, Mar. Pet. Geol. 22 (2005) 375–390.
[19] L. Hou, K. He, J. Zhai, J. Mi, N. Weng, Compositional kinetics for hydrocarbon evolution in the pyrolysis of the chang 7 organic matter: implications for in-situ conversion of oil shale, J. Anal. Appl. Pyrolysis 162 (2022), 105434.
[20] Y. Wang, X. Han, Z. Gao, X. Jiang, Thermal cracking of the large molecular alcohols in shale oil by experimental study and kinetic modeling, J. Anal. Appl. Pyrolysis 168 (2022), 105749.
[21] M. Wang, S. Lu, H.X. Xue, Kinetic simulation of hydrocarbon generation from Lacustrine Type I Kerogen from the Songliao Basin: model comparison and geological application, Mar. Pet. Geol. 28 (2011) 1714–1726.
[22] Z. Wei, Y. Zou, Y. Cai, L. Wang, X. Luo, Kinetics of oil group-type generation and expulsion: an integrated application to dongying depression, Bohai Bay Basin, China, Org. Geochem. 52 (2012) 1–12.
[23] Z. Wang, Y. Tang, Y. Wang, Y. Zheng, F. Chen, S. Wu, D. Fu, Kinetics of shale oil generation from kerogen in saline basin and its exploration significance: an example from the eocene qianjiang formation, Jianghan Basin, China, J. Anal. Appl. Pyrolysis 150 (2020), 104885.
[24] P. Sundararaman, P.H. Merz, R.G. Mann, Determination of Kerogen activation energy distribution, Energy Fuels 6 (1992) 793–803.
[25] K.E. Peters, A.K. Burnham, C.C. Walters, Petroleum generation kinetics: single versus multiple heating-ramp open-system pyrolysis, AAPG Bull. 99 (2015) 591–616.
[26] F. Froidl, L. Zieger, N. Mahlstedt, R. Littke, Comparison of single-and multi-ramp bulk kinetics for a natural maturity series of Westphalian coals: implications for modelling petroleum generation, Int. J. Coal Geol. 219 (2020), 103378.
[27] K.E. Peters, A.K. Burnham, C.C. Walters, O. Schenk, Guidelines for kinetic input to petroleum system models from open-system pyrolysis, Mar. Pet. Geol. 92 (2018) 979–986.
[28] S. Inan, H.J. Schenk, , Evaluation of petroleum generation and expulsion from a source rock by open and restricted system pyrolysis experiments. Part I. Extrapolation of experimentally-derived kinetic parameters to natural systems, J. Anal. Appl. Pyrolysis 58 (2001) 213–228.
[29] L.M. Johnson, R. Rezaee, G.C. Smith, N. Mahlstedt, D.S. Edwards, A. Kadkhodaie, H. Yu, Kinetics of hydrocarbon generation from the marine ordovician goldwyer formation, Canning Basin, Western Australia, Int. J. Coal Geol. 232 (2020), 103623.
[30] D. Chen, X. Pang, L. Li, F. Jiang, G. Liu, M. Li, B. Pang, H. Jiang, Z. Xu, W. Han, Organic geochemical characteristics and shale oil potential of the middle eocene early-mature shale in the Nanpu Sag, Bohai Bay Basin, Eastern China, Mar. Pet. Geol. 133 (2021), 105248.
[31] F. Hao, X. Zhou, Y. Zhu, H. Zou, X. Bao, Q. Kong, Mechanisms of petroleum accumulation in the Bozhong Sub-basin, Bohai Bay Basin, China. Part 1: origin and occurrence of crude oils, Mar. Pet. Geol. 26 (2009) 1528–1542.
[32] F. Hao, X. Zhou, Y. Zhu, H. Zou, Y. Yang, Charging of oil fields surrounding the shaleitian uplift from multiple source rock intervals and generative kitchens, Bohai Bay Basin, China, Mar. Pet. Geol. 27 (2010) 1910–1926.
[33] F. Jiang, X. Pang, J. Bai, X. Zhou, J. Li, Y. Guo, Comprehensive assessment of source rocks in the Bohai Sea Area, Eastern China, AAPG Bull. 100 (2016) 969–1002.
[34] C. Xu, H. Yu, J. Wang, X. Liu, Formation conditions and accumulation characteristics of Bozhong 19-6 large condensate gas field in offshore Bohai Bay Basin, Pet. Explor. Dev. 46 (2019) 27–40.
[35] F. Jiang, X. Pang, Quantitative evaluation of hydrocarbon resource potential and its distribution in the Bozhong Sag and surrounding areas, Bohai Bay Basin, Pet. Explor. Dev. 38 (2011) 23–29.
[36] F. Hao, X. Zhou, Y. Zhu, Y. Yang, Lacustrine source rock deposition in response to co-evolution of environments and organisms controlled by tectonic subsidence and climate, Bohai Bay Basin, China, Org. Geochem. 42 (2011) 323–339.
[37] G. Li, C. Liu, F. Wang, G. Tang, H. Yang, X. Zeng, Y. Wu, X. Yang, Geochemical characteristics and hydrocarbon generation mode of source rocks of dongying formation in Bozhong Sag, Bohai Bay Basin, Acta Pet. Sin. 43 (2022) 1568–1584.
[38] Z. Gong, W. Zhu, P.P. Chen, Revitalization of a mature oil-bearing basin by a paradigm shift in the exploration concept. A case history of Bohai Bay, Offshore China, Mar. Pet. Geol. 27 (2010) 1011–1027.
[39] M.B. Allen, D. Macdonald, Z. Xun, S.J. Vincent, C. Brouet-Menzies, Early cenozoic two-phase extension and late cenozoic thermal subsidence and inversion of the Bohai Basin, Northern China, Mar. Pet. Geol. 14 (1997) 951–972.
[40] J. Ren, K. Tamaki, S. Li, Z. Junxia, Late Mesozoic and Cenozoic rifting and its dynamic setting in eastern china and adjacent areas, Tectonophysics 344 (2002) 175–205.
[41] Q. Liu, L. He, L. Chen, Tectono-thermal modeling of Cenozoic multiple rift episodes in the Bohai Bay Basin, Eastern China and its geodynamic implications, Int. J. Earth Sci. 107 (2018) 53–69.
[42] B. Pasaribu, C. Chen, Y.K. Liao, P. Jiang, J.T. Tzen, Identification of Caleosin and Oleosin in oil bodies of pine pollen, Plant Physiol. Biochem. 111 (2017) 20–29.
[43] E. Hwang, K. Ki, H. Chung, Proximate composition, amino acid, mineral, and heavy metal content of dried laver, Prev. Nutr. Food Sci. 18 (2013) 139.

[44] S. Arrhenius, Über die reaktionsgeschwindigkeit bei der inversion von rohrzucker durch säuren, Z. für Phys. Chem. 4 (1889) 226–248.
[45] W. Zhu, L. Mi, Z. Gong, Reservoir Formation and Petroleum Exploration in Bohai Sea, Science Press, Beijing, 2009.
[46] R.F. Li, G.X. Zhang, X.F. Ruan, Study on the recovery of erosion quantity of unconformities of Paleogene-neogene in Bohai sea area, Geol. Rev. 58 (2012) 542–552.
[47] T. Hantschel, A.I. Kauerauf, Fundamentals of Basin and Petroleum Systems Modeling, Springer Science & Business Media, 2009.
[48] H. Yang, C.L. Liu, F.L. Wang, G.M. Tang, G.X. Li, X.X. Zheng, Y.P. Wu, Paleoenvironment and development model of source rocks of dongying formation in Bozhong Sag, Lithol. Res. 33 (2021) 81–92.
[49] B. Wygrala, Integrated Study of an Oil Field in the Southern Po Basin, Northern Italy, University of Cologne, Germany, 1989.
[50] S. Hu, P.B.O. Sullivan, A. Raza, B.P. Kohn, Thermal history and Tectonic subsidence of the Bohai Basin, Northern China: a cenozoic rifted and local pull-apart basin, Phys. Earth Planet. Inter. 126 (2001) 221–235.
[51] N.S. Qiu, G. Wei, C.C. Li, Y. Zhang, Y.H. Guo, Distribution features of current geothermal field in the Bohai Sea waters, Oil & Gas Geol. 30 (2009) 412–419.
[52] N. Qiu, W. Xu, Y. Zuo, J. Chang, Meso–cenozoic thermal regime in the Bohai Bay Basin, Eastern North China craton, Int. Geol. Rev. 57 (2015) 271–289.
[53] K.S. Jackson, P.J. Hawkins, A. Bennett, Regional facies and geochemical evaluation of the Southern Denison Trough, Queensland, APPEA J. 20 (1980) 143–158.
[54] R.S. Awan, C. Liu, N. Aadil, Q. Yasin, A. Salaam, A. Hussain, S. Yang, A.K. Jadoon, Y. Wu, M.A. Gul, Organic geochemical evaluation of Cretaceous Talhar shale for shale oil and gas potential from lower Indus Basin, Pakistan, J. Pet. Sci. Eng. 200 (2021), 108404.
[55] Y. Wu, C. Liu, F. Jiang, T. Hu, J. Lv, C. Zhang, X. Guo, L. Huang, M. Hu, R. Huang, Geological characteristics and shale oil potential of alkaline lacustrine source rock in fengcheng formation of the Mahu Sag, Junggar Basin, Western China, J. Pet. Sci. Eng. 216 (2022), 110823.
[56] M.H. Hakimi, A.F. Ahmed, Organic-geochemistry characterization of the Paleogene to Neogene source rocks in the Sayhut Subbasin, Gulf of Aden Basin, with emphasis on organic-matter input and petroleum-generation potential, AAPG Bull. 100 (2016) 1749–1774.
[57] G. Skarstein, S. Ohm, A. Cedeno, A. Escalona, Facies variations in the upper Jurassic source rocks of the Norwegian North Sea: from micro-to macro scale, Mar. Pet. Geol. 145 (2022), 105856.
[58] K.E. Peters, M.R. Cassa, Applied source rock geochemistry: chapter 5: part ii. Essential elements, AAPG Bull. 70 (1994) 93–120.
[59] D.M. Jarvie, B.L. Claxton, F. Henk, J.T. Breyer, Oil and shale gas from the Barnett Shale, Ft. Worth Basin, Texas, AAPG Natl. Conv. Am. Assoc. Pet. Geol. Denver, Colo. (2001) A100.
[60] D.M. Jarvie, Petroleum systems in the Permian Basin: targeting optimum oil production, Houst. Geol. Soc. Bull. 60 (2018) 27.
[61] R.J. Drozd, Adventures in pyrolysis ii, modeling pyrolysis peaks of petroleum source rocks, J. Anal. Appl. Pyrolysis 142 (2019), 104385.
[62] S. Yang, H. Wang, J. Zheng, Y. Pan, C. Ji, Comprehensive review: study on heating rate characteristics and coupling simulation of oil shale pyrolysis, J. Anal. Appl. Pyrolysis (2023), 106289.
[63] D. Mani, D.J. Patil, A.M. Dayal, B.N. Prasad, Thermal maturity, source rock potential and kinetics of hydrocarbon generation in permian shales from the Damodar Valley Basin, Eastern india, Mar. Pet. Geol. 66 (2015) 1056–1072.
[64] D.W. Houseknecht, D.O. Hayba, Modeling oil generation in the undeformed part of the Arctic national wildlife refuge 1002 area, U. S. Geol. Surv. 98 (1998) 1–24.
[65] L. Lan, Y. Li, K. Wang, X. Jiang, T. Sun, J. Wang, Biomarker parameters for effectively distinguishing source rocks in Bozhong Sag, Acta Pet. Sin. 40 (2019) 35–41.